7-15-2022

Coupling ^{210}Pb and ^{14}C to constrain carbon burial efficiency of blue carbon ecosystems

Tynisha R. Martin
University of South Florida

Coupling ^{210}Pb and ^{14}C to Constrain Carbon Burial Efficiency of Blue Carbon Ecosystems

by

Tynisha R. Martin

A thesis submitted in partial fulfillment
of the requirements for the degree of
Master of Science in Marine Science
with a concentration in Geological Oceanography
College of Marine Science
University of South Florida

Major Professor: Brad Rosenheim, Ph.D.
Ryan P. Moyer, Ph.D.
Joseph M. Smoak, Ph.D.
Nancy Williams, Ph.D.

Date of Approval:
July 15, 2022

Keywords: blue carbon, Ten Thousand Islands, Charlotte Harbor, carbon cycling

DEDICATION

For my nephew Jahlil – you can do anything you set your mind to.

For my mom, my backbone and the strongest person I know.

ACKNOWLEDGMENTS

I would like to start by thanking my advisor, Dr. Brad Rosenheim, for his continual guidance throughout this experience. He supported me through my schoolwork and my personal struggles, always there to listen and not judge. Though at times I felt like he was speaking another language to me, I am glad that he didn't give up on me. Thanks to my committee for their guidance and continual edits. Thank you for pushing me to question my work and think about how to make my writing stronger.

The support I have received from my lab mates has undoubtedly helped my career as a graduate student. Whether they were there to read drafts, teach me new software, or offer a shoulder to cry on – I always felt like I had a place to go. To Ryan and Carey for always listening to me vent, and providing any support I needed, you guys don't know how much it meant to me. To Kiersten, we came in together and have been through everything together – I think it will be weird leaving you. To Theresa, thank you for always reading my writing and providing me honest, constructive feedback, and for offering advice when you knew I needed it most. To Thea and Orion, thank you for your help with my writing – my thesis wouldn't be as well-written, and I wouldn't be as strong of a scientist without you. To those who were there to help with my code when I was clueless – there is no way I would have been able to do this without your guidance.

To my family: I am eternally grateful for the support I have received from all of you. My parents raised me to go for my dreams, and for a while I wasn't sure what my dreams were. They supported me anyway. Mom taught me to be independent and question the world around me. My

dad taught me to be strong and never quit. To my sister, Kelsey, thank you for being my sounding board and talking me off the ledge multiple times. Jahlil, you have kept me sane.

To my friends who have taken this journey with me, thank you for being there. To MK, who has almost single-handedly kept me afloat the last year: thank you and Dante for doggie calls to make me smile and focus. To Nikki and Jayme: thank you for spending the good times with me and pushing me through the hard times. To Hannah: thank you for being a sounding board and going through this whole experience with me. To anyone I haven't mentioned by name, your support was monumental in getting me to this point and I am grateful.

Lastly to my cat Oliver: you have been my emotional support and entertained everyone in lab meetings. Thank you for being an unmentioned co-author.

TABLE OF CONTENTS

LIST OF TABLES

LIST OF FIGURES

ABSTRACT

Blue carbon ecosystems cover a small global area but have the potential to sequester large amounts of organic carbon (OC) from the coastal ocean in the sediment. Organic carbon is continually remineralized and exported in the dissolved form, which is currently only poorly accounted for in blue carbon budgets. Constraining carbon cycling in blue carbon systems is complicated by the range of carbon sources and sinks in the system and high export rates from the system. By coupling ^{14}C and ^{210}Pb chronometers to ascertain the amount of primary production stored within peat, it is possible to study carbon transport through peat systems and examine first order changes in carbon stock through time. Peat cores were collected from three sites in the Charlotte Harbor and Ten Thousand Islands regions of Southwest Florida. Within the top 25 cm of core, the ^{210}Pb chronology extends to different age maxima in each system, from 1937 CE in the salt marsh system to 1892 CE in the riverine mangrove system. Radiocarbon dates for all systems indicate modern deposition. By coupling independent chronometers ^{210}Pb and ^{14}C, I was able to determine an age-depth relationship while also tracing the movement of younger carbon from the surface to depth downcore.

To better understand the mechanisms and dynamics of carbon sequestration in these ecosystems, a simplified advection model was constructed to visualize the differences in concentrations of OC at differing depths. Different sensitivity tests were conducted to determine the sensitivity of the model to the method of downward carbon transport. The salt marsh system had the smallest carbon mixing depth (25 years) and proportion (0.2) and highest export value (0.6). Conversely, the basin mangrove system has the deepest mixing depth (120 years) but the

lowest export value (0.5). I was unable to fit the data sets from this study to the atmospheric bomb curve, despite the addition of a reactive loss term. I assumed all carbon exported was in the form of DIC and did not control for other speciation, which implies that the DIC is likely an overestimate. My results show that the amount of carbon stored in the basin mangrove system (80.11 Mg C ha^{-1}) was an order of magnitude lower than the riverine mangrove system (691.75 Mg C ha^{-1}), but higher than that in salt marsh systems (59.03 Mg C ha-1). Assuming the cores taken are indicative of the system, riverine mangroves in the Ten Thousand Islands store 5.04 x 10^6 Mg of carbon in the soil. Making the same assumption, the amount of carbon stored in the Ten Thousand Islands basin mangrove system is an order of magnitude lower at 5.83 x 10^5 Mg. Salt marsh systems in Charlotte Harbor store 3.5 x 10^5 Mg of carbon in the sediment. Peats in the Ten Thousand Islands have been dated at 3,500 years. During the time since peats have been forming in the Ten Thousand Islands, there has been 4.89 x 10^8 Mg C of carbon produced. In Charlotte Harbor, peats have been forming for 2,180 years. During this time, 2.31 x 10^8 Mg C of carbon has been produced.

When I compared the amount of carbon produced to the amount of carbon stored, the percent of carbon stored is exceedingly small (<1.05%). The quantities of carbon produced and stored were used as a marker for comparison to the model. These calculations also helped to provide some nuance as to how the inefficiency in the systems occurs. Whereas some carbon is stored in the system, more is exported from the system than is stored, making the system inefficient. Previous research has suggested that blue carbon ecosystems experience efficient carbon sequestration, but many lose a significant fraction of net primary production to coastal waters. Carbon sequestration in blue carbon systems doesn't meet the definition of efficiency that was used in this study, as my results indicate that a substantial portion of the carbon in the system

is lost or exported as DIC. My results indicate that blue carbon systems are effective in sequestering CO_2 from that atmosphere, but not efficient in burying it in long-term storage.

CHAPTER ONE:

INTRODUCTION

1.1 Coastal Wetland Services

Coastal wetlands occupy a substantial portion of the coastline globally (Himes-Cornell et al., 2018) but only cover 4 – 6% of Earth's land area (Mitra et al., 2005). A combination of the geomorphology, vegetation, and habitat conditions allow coastal wetlands to provide several important ecological services, including coastline protection, greenhouse gas reduction, water filtration, carbon storage, and sediment trapping. Any native vegetation within the first kilometer of the coastline has adapted to survive in a dynamic environment where rapid migration of sediment after disturbances and episodic conditions of salt water inundation occur (Feagin et al., 2010). These adaptations allow the vegetation – particularly mangroves – to shield the coastline from any damage that may come from storms or floods, while also stabilizing the sediments within the system. Utilizing extensive root systems, coastal wetlands promote sedimentation by slowing water flow and trapping sediment around the vegetation. This trapping of particles prevents sediment resuspension into the water column and leads to accretion (Mazda et al., 2005; Lee et al., 2014). Coastal wetlands act as sinks for organic carbon (OC) that is synthesized from greenhouse gases, using the photosynthetic uptake of atmospheric carbon dioxide (CO_2) to store OC as biomass or sequester OC in the sediment (Jennerjahn & Ittekkot, 2002; Poffenbarger et al., 2011; Smoak et al., 2013). By removing carbon from Earth's surface, the sequestration process enhances atmospheric O_2 accumulation and CO_2 removal (Hemingway et al., 2019).

The ability of coastal wetlands to sequester carbon from the atmosphere naturally is an ecosystem service that can often be overlooked, partially due to the uncertainty of how effective they are at carbon sequestration. The term blue carbon was established to describe these coastal wetland ecosystems (Nellemann et al., 2009; Macreadie et al., 2019), which include mangroves, salt marshes and seagrass habitats. The amount of carbon sequestered in mangrove and salt marsh sediments can range depending on vegetation and tidal range (Mcleod et al., 2011). Blue carbon ecosystems are among the most carbon-rich biomes in the world, with mangroves having a carbon stock twice as large as salt marshes (Alongi, 2012; Chatting et al., 2020) (Table 1 & Fig. 1). Whereas salt marshes range from arctic to subtropical climates globally (Chmura et al., 2003), mangroves are generally concentrated around 25 °N to 25 °S (Chmura et al., 2003; Murray et al., 2015), where they largely replace salt marshes. Some research suggests that the capacity for salt marsh carbon sequestration is higher than that of mangroves, and that the carbon budget for salt marshes is smaller due to their smaller and declining global area (Bianchi et al., 2013; Ouyang & Lee, 2013, 2014).

Table 1. *Above- and belowground (roots) biomass, soil carbon stock, and net primary production (NPP) of salt marsh and mangrove systems. All values are in units of Gg C km^{-2} (Pendleton et al., 2012; Alongi, 2014, 2020a; Reithmaier et al., 2021).*

System	Aboveground Biomass	Belowground Biomass	Soil Stock (to 1 m depth)	Aboveground NPP	Belowground NPP
Mangrove	12.39	7.51	60.79	1.32	0.52
Salt Marsh	0.75	2.80	40.07	0.5	1.26

Belowground carbon storage is often difficult to quantify because it incorporates thousands of years of variable deposition, transformation, and erosion dynamics associated with fluctuating sea level and episodic disturbances (Donato et al., 2011). There is a large pool of carbon stored in dead roots that helps to conserve and recycle nutrients within the sediment (Alongi, 2014).

Nutrients in salt marshes stimulate aboveground production, often at the expense of belowground allocation, and could cause a slowing of organic matter (OM) accumulation (Turner et al., 2009; Spivak et al., 2019). The root and rhizome biomass can diminish with nutrient enrichment as plants adjust foraging strategies, which may lead to lower soil organic content (Turner et al., 2009). Tidal range plays an important role in belowground carbon dynamics, including carbon burial and root production by affecting sediment aeration and porewater flow (Ouyang & Lee, 2013). This also affects organic matter import and export dynamics within the blue carbon ecosystem (Ouyang & Lee, 2013).

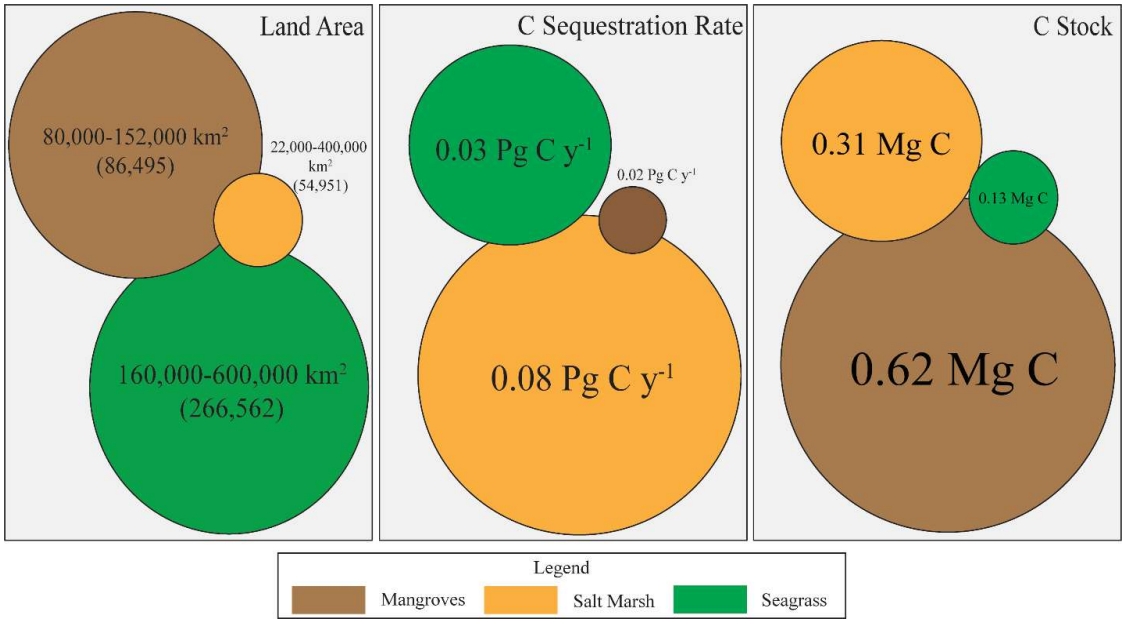

Figure 1. *Summary of global scale estimates of blue carbon ecosystems from literature. Land area in parentheses indicates the most recent average. C sequestration rate incorporates burial rate. C stock is measured within the top 1 m of sediment (Mcleod et al., 2011; Alongi, 2012; Pendleton et al., 2012; Alongi, 2014; Duarte, 2017; McKenzie et al., 2020; Alongi, 2020a; Reithmaier et al., 2021).*

1.2 Blue Carbon System Formation

Blue carbon ecosystems are populated by halophytes, plants that have adapted to survive in saline environments despite the high concentrations of electrolytes in the environment (Flowers

et al., 1977). To accomplish this, halophytes must maintain a sufficient level of freshwater in their cells so that metabolic function may continue against the higher osmotic pressure occurring inside the soil (Feller et al., 2010). The tolerance of halophytic vegetation to salinity depends on the synthesis of compatible organic solutes and the controlled uptake and compartmentalization of Na^+, K^+, and Cl^- ions within the cells and tissues of the plant (Flowers & Colmer, 2008). The structural complexity of blue carbon ecosystems – the root structure, leafy canopies, and dense vegetation – allow them to exist along a gradient of physical and chemical settings (Alongi, 2012). Tidal elevation gradients occur within blue carbon ecosystems, where seagrasses are continuously submerged but salt marsh and mangrove systems exist subaerially. Several changes occur within the system because of tidal elevation, including microbial processes, vegetation species and density, sediment structure, and soil carbon accumulation rates (Chmura et al., 2003; Mazda et al., 2005; Kristensen et al., 2008b; Turner et al., 2009; Chambers et al., 2016; Rosentreter et al., 2018b; Spivak et al., 2019). Chemical gradients, such as salinity, redox potential, and soil ionic composition, exist within wetlands and further demonstrate the ability of the vegetation to adapt to varying conditions (Christian et al., 1990; Lee & Kim, 2018).

1.2.1 Mangrove Forests

Mangroves are the only woody halophytes that can survive in the saltwater along the world's subtropical and tropical coasts (Alongi, 2012). As such, mangroves have developed many structural and functional adaptations which help them to survive in an ever-changing environment. Mangroves possess viviparous embryos, aerial roots that enable them to respire in anoxic and waterlogged soil, and many physiological mechanisms which help tolerance of saltwater conditions (Alongi, 2012). The seeds, or propagules, of the red mangrove, *Rhizophora mangle,*

float so that they are transported by tidal currents to intertidal areas where they may take root and live (Shier, 1969). Once established, the roots of adjacent trees can become intertwined and collect any floating debris or sediment, thus allowing for sedimentation buildup (Shier, 1969). The pneumatophores of the black mangrove, *Avicennia germinans*, also allow for sedimentation by causing turbulent wakes around them during high tide (Alongi, 2012), which causes sediment suspension until slack water.

Mangroves have a higher below- to above-ground carbon mass ratio and allocate more carbon belowground proportionally than terrestrial trees (Komiyama et al., 2008; Alongi, 2012). Much of the belowground carbon is stored in dead root biomass (Berner & Raiswell, 1983), which can serve as a nutrient conserving mechanism for the tree (Alongi, 2012), or in the soil. A large pool of belowground root biomass combined with the carbon-rich soil may be indicative of the numerous morphological and physiological adaptations of mangroves to life in a harsh, saline waterlogged environment (Alongi, 2012). The persistence of mangroves over geologic time is thought to be a result of the greater carbon investment in the roots and the annual root production of the tree (Feller et al., 2010).

Mangroves cope with the saturated environment through the highly diverse and productive microbial assemblages that reside in the soils (Alongi, 2005), through which the bulk of mangrove carbon is processed (Lee et al., 2014). All mangrove soils have a suboxic peat layer that is variably thick and tidally submerged, which sustain anaerobic decomposition pathways (Donato et al., 2011). Peat formation in mangroves occurs from the deposition and slow turnover of roots as aboveground tissues decay and are transported throughout the system (Chmura et al., 2003). Peats typically consist of root fragments and fine roots (Ouyang et al., 2017). Mangroves are generally

threatened by coastal disturbance and pollution, land-use change, and upstream soil loss (Alongi, 2012; Himes-Cornell et al., 2018).

1.2.2 Salt Marsh Habitats

Salt marshes are intertidal grasslands that form along temperate, sheltered coastlines, continental margins, and in bays and estuaries. They are prominent in passive continental margins and develop in areas with subdued wave action (Flowers & Colmer, 2008). A flat shoreline that is protected from waves is necessary for pioneer vegetation as the water needs to be calm enough for seeds to germinate (Friedrichs & Perry, 2001). If the area is inundated too frequently or for a prolonged period, waterlog will occur and the grasses will not survive. Once establishment occurs, the conditions for net deposition increase dramatically and salt marshes will accrete rapidly both vertically and horizontally (Friedrichs & Perry, 2001). Sediment is brought into the system via tides and trapped by vegetation, further aiding in accretion (Drake et al., 2015). Vertical accretion in organic-rich salt marshes is driven by organic material accumulation, largely through allochthonous plant litter inputs and root and rhizome contributions (Chmura & Hung, 2004; Turner et al., 2009). Peat accumulation occurs within the system as a means of maintaining elevation within the tidal frame (Gerlach et al., 2017). Salt marshes have been impacted by sea-level rise, pollution, marsh reclamation and vegetation disturbance, and altered hydrological regimes (Beaumont et al., 2014; Himes-Cornell et al., 2018).

Salt marshes are characterized by a sharp zonation of plants and low species diversity, but very high production (Himes-Cornell et al., 2018). Different zones within the marsh are home to differing species of salt marsh grasses largely due to tidal inundation frequency. Salt marsh plants have salt hairs and salt glands, the ability to adjust osmotically, and selective ion uptake abilities

(Flowers et al., 1977; Flowers et al., 1986; Ungar, 1998; Lee & Kim, 2018), which allow them to exist in these environments. Grasses sequester CO_2 from the atmosphere and store it in living plant tissue (Caçador et al., 2004), leading to high productivity (Martinetto et al., 2016). Like mangroves, salt marshes have a high capacity for carbon sequestration in the soil. A large portion of the soil OC (SOC) is derived from roots (Redelstein et al., 2018), with certain species, such as *Spartina maritima*, having larger root decay rates than others, like *Juncus spp.* (Ouyang et al., 2017). In the salt marsh, unlike in mangroves, aboveground litter is more readily decayed than roots due to the oxygen availability and chemical composition differences (Ouyang et al., 2017). Like mangroves, *Spartina spp.* aerates the sediment through its root system (Ouyang et al., 2017).

1.2.3 Accretion in Blue Carbon Systems

The hydrodynamics, mediated by biological properties of the system, control the degree of particle trapping that allows the vegetation to sequester carbon from outside ecosystem boundaries (Gacia & Duarte, 2001; Mcleod et al., 2011; Hansen & Reidenbach, 2012; Wilkie et al., 2012; Macreadie et al., 2019). The proficiency of blue carbon ecosystems to trap particulate matter is often dependent on tidal pumping, salinity, areal extent of the intertidal zone, and particle size (Wolanski, 1995; Kristensen et al., 2008b). Accretion occurs through litter deposition, as well as accumulation of sediment imported?? from the daily tides that is trapped by the vegetation in the system (Twilley et al., 1992; Pendleton et al., 2012; Drake et al., 2015). Sediments are delivered through riverine or longshore-tidal transport and storm-surge events and accumulate around the vegetation, leading to increases in surface elevation (Breithaupt et al., 2017; Breithaupt et al., 2019; Spivak et al., 2019). Vertical accretion is largely dependent on the balance between any OM inputs into the system and carbon loss from the system (Pendleton et al., 2012; Chambers et al., 2013).

An increase in tidal inundation depth allows additional allochthonous sediment to enter the system, enhancing vertical accretion and plant productivity. Vertical accretion within the system is primarily results from an accumulation of organic materials, rather than inorganic materials (Turner et al., 2009). Allochthonous particle deposition has been shown to increase soil elevation while stabilizing OM against decomposition (Spivak et al., 2019) and diminish SOC loss rates (Chambers et al., 2016).

1.3 Bioturbation

Bioturbation enhances in the decomposition of OM (Martinetto et al., 2016) and downward transport of carbon (Kristensen, 2008a) within blue carbon ecosystems. Because blue carbon habitats are so carbon-rich, nutrients and O_2 are depleted quickly to support the microbial food chain. Bioturbation works to returns these reactants to the system and maintain microbial function. Fissures, cracks, burrows, tubes, drainage channels, and extensive roots through which tidal waters can percolate and drain (Alongi, 2020b) are integral parts of a productive system. The connectivity of burrows within the system enhances porewater exchange (Santos et al., 2019) and increases the area of sediment available for sediment-water biogeochemical exchange (Santos et al., 2021). As a result, the transport of solutes via tidal pumping, an advective process, is much faster than molecular diffusion (Santos et al., 2021).

Nearshore sediments support large populations of burrowing macroinfauna, such as crabs, polychaete worms, and shrimps (Koretsky et al., 2002). These organisms build extensive burrow networks that increase the sediment area available for biogeochemical exchange, allowing for higher rates of advection to occur (Bouillon et al., 2007; Santos et al., 2021). As bioturbating organisms exhume older material out of the burrow and deposit fresh detrital material along the

burrow (Kristensen et al., 2008b), large quantities of remineralized nutrients are accumulated and concentrated in the water within the burrows (Martinetto et al., 2016). Remineralized nutrients and metabolic products are delivered to the sediment-water interface via porewater exchange or tidal pumping (Santos et al., 2019; Reithmaier et al., 2020).

Whereas crab burrows are confined to the upper 1 m of sediment (Koretsky et al., 2002; Martinetto et al., 2016), roots have the largest effect below this depth in the sediment. Living root biomass is contained within the upper 0–40 cm of soil (Alongi, 2012) but the pool of dead roots can extend to a much greater depth. The soil is aerated through roots and peats often consist of fine roots and root fragments (Ouyang et al., 2017). Oxygen is transported to the soil through the root system, stimulating the root community and maintain high redox conditions in the rhizosphere (Kristensen & Alongi, 2006; Chambers et al., 2016). Labile carbon is stabilized by root exudates and transported in the dissolved phase through porewater advection (Schafer, 2020). The exudation of labile DOC from the root system stimulates heterotrophic CO_2 generation within the sediment (Kristensen & Alongi, 2006).

In addition to bioturbation, root production can account for up to one third of primary productivity of blue carbon ecosystems. The remaining production is divided between aboveground litter and wood production (Alongi et al., 2003; Alongi et al., 2004; Alongi, 2014). Sequestered carbon is stored in living biomass above- and belowground, in nonliving biomass belowground, and in sediment (Mcleod et al., 2011). It is thought that litterfall provides the dominant OC input in the sediment (Bouillon et al., 2008; Kristensen et al., 2008b). Coastal eutrophication leads to higher accumulation of inorganic matter in the aboveground vegetation, which, in turn, can cause a decline in belowground biomass production and lower soil OC content (Spivak et al., 2019).

1.4 Blue Carbon and the Carbon Cycle

Organic carbon is constantly remineralized and exported as dissolved carbon, which is currently only poorly accounted for in blue carbon budgets (Reithmaier et al., 2020). Mangroves respire 75% of the carbon that they take up back into the atmosphere (Twilley, 1985; Najjar et al., 2018; Macreadie et al., 2019), and are responsible for 13% and 28% of global dissolved organic and inorganic carbon (DOC and DIC, respectively) outwelling to the coastal ocean, respectively (Bouillon et al., 2008; Alongi, 2020b; Santos et al., 2021). This lateral outwelling accounts for <3% OC loss from the system (Alongi, 2012; Chambers et al., 2013; Martinetto et al., 2016; Santos et al., 2021). Carbon burial in salt marsh sediments is ~20% of the atmospheric CO_2 uptake by vegetation, with almost all of it buried as OC (Santos et al., 2021). The lateral exchange of carbon and alkalinity is thought to be a large sink to the coastal ocean (Maher et al., 2018; Reithmaier et al., 2020; Santos et al., 2021). Any OM that is not exported to the coastal ocean will enter the sediment to be consumed, degraded, and chemically modified by microbes (Kristensen et al., 2008b).

1.4.1 Carbon Cycle Constraints

Constraining carbon cycling – including reservoir and flux sizes – in blue carbon ecosystems is complicated by the difficulty of obtaining direct measurements and the diversity of carbon sources and sinks (Fig. 2). The most common methods for measuring system fluxes include static chambers and discrete water samples, laboratory incubation, and spectroscopy analysis (Kadlec, 2000; Murray et al., 2015; Rosentreter et al., 2018b). These measurements can be complicated by disturbances (Mcleod et al., 2011; Smoak et al., 2013; Alongi, 2014; Breithaupt et

al., 2019), seasonal rainfall amounts (Twilley, 1985; Macreadie et al., 2019), and salinity fluctuations (Poffenbarger et al., 2011). Flux data is often upscaled using global blue carbon ecosystem area but can also be scaled to account for the local system in which the measurements were taken (Maher et al., 2016; Rosentreter et al., 2018b).

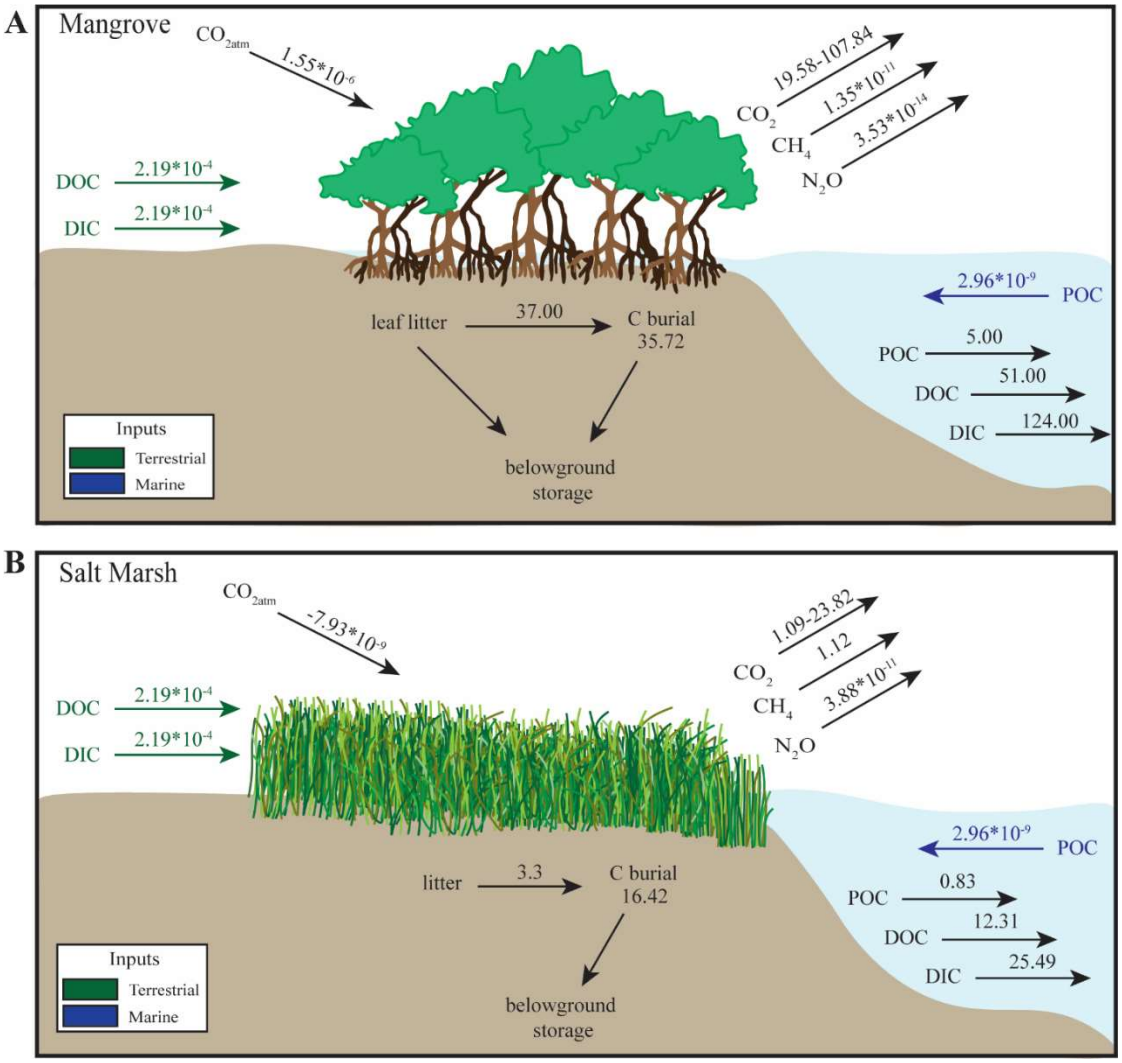

Figure 2. *Conceptual model of carbon influx and efflux to A) mangrove and B) salt marsh systems, calculated using values reported by the noted studies. Values are in units of Tg C y^{-1} and are normalized to estimated land area. This study focused on dissolved organic carbon (DOC), dissolved inorganic carbon (DIC), particulate organic carbon (POC), methane (CH_4), and nitrous oxide (N_2O)(Duarte et al., 2005; Mcleod et al., 2011; Pendleton et al., 2012; Saintilan et al., 2013; Duarte, 2017; Alongi, 2020a; Rosentreter et al., 2021; Santos et al., 2021; Wang et al., 2021).*

Estimating outwelling and efflux involves measuring geochemical tracers, including radon and radium, over tidal cycles and transects across the continental shelf (Maher et al., 2013; Sippo et al., 2017; Cabral et al., 2021). There is a lack of estimates over differing spatial scales, which makes it difficult to fully constrain blue carbon budgets (Cabral et al., 2021). Further, there seems to be "missing carbon" from the budget, which studies have been attempting to explain for years (Chen et al., 2012; Maher et al., 2013; Leopold et al., 2015; Lovelock et al., 2015; Ouyang et al., 2017; Ray et al., 2018). Specifically, little is known about DIC in blue carbon budgets (Lee et al., 2014) but it could be the "missing carbon". The export of DIC to the coastal ocean is believed to be the largest sink of atmospheric greenhouse gases (Maher et al., 2018). However, fluxes of potent greenhouse gases, such as methane (CH_4) and nitrous oxide (N_2O), and lateral carbon export are often overlooked in the blue carbon budgets (Maher et al., 2018). Measuring the magnitude of lateral carbon export can be complicated by the high temporal variability of biogeochemical, hydrological, and physical processes within the system (Chu et al., 2018).

1.4.2 System Fluxes

Blue carbon systems support several in- and effluxes, which allow nutrients and materials to cycle through the system. Terrestrial OM (TOM) is added to the system through wood production and leaf litter (Twilley, 1988; Twilley et al., 1992). TOM will either be exported tidally or will decompose *in situ* and be stored in the sediment. Upon decomposition, TOM will either become dissolved or particulate organic carbon (POC). DOC is sourced from the primary production in the system and any detritus from the organisms living in blue carbon ecosystems. In addition to autochthonous decay, DOC can be tidally imported into the system (Twilley, 1988; Twilley et al., 1992; Maher et al., 2013). Porewater exchange is a minor source of DOC (Sippo et

al., 2017), with release through root exudates (Kristensen et al., 2008b) into the soil. Root exudates are thought to be a source of young carbon to the system (Schafer, 2020). DOC is flushed out of the system via the tides as well as released from detritus and leaves in the water column (Dittmar et al., 2006). The biogeochemical cycling of DIC is controlled by plant production and microbial activity, including respiration (Chu et al., 2018). Soil DIC production occurs in both mangrove and salt marsh systems, with mangrove production (18.27 ± 2.3 Mg ha^{-1}) being larger than salt marsh production (6.92 ± 1.61 Mg ha^{-1}) (Alongi, 2020a, 2020b).

Efflux of DIC may be a substantial long-term carbon sink (Maher et al., 2018) to the coastal ocean. It has also been suggested the DIC outwelling is sustained by porewater or groundwater inputs (Santos et al., 2021), with porewater-derived DIC export being considered a major carbon export pathway globally (Maher et al., 2017). Like DOC, POC can also be tidally imported (Twilley, 1988; Twilley et al., 1992; Maher et al., 2013) but is primarily sourced from the autochthonous breakdown of OM. The influx of POC from the marine environment supports mineralization within the system (Bouillon et al., 2007). DOC and POC are also exported by tides to be either deposited on the continental shelf or deep ocean or be eaten or mineralized offshore (Alongi, 2012; Duarte, 2017). Mangroves export two times more DOC and three times more POC and DIC to adjacent coastal waters than salt marshes (Santos et al., 2021).

Blue carbon soils are a source of microbially-mediated gases, such as CO_2, CH_4, and N_2O, to the atmosphere (Alongi, 2005). High fluxes of CO_2 have been attributed to sedimentary metabolic activity and the efficient exchange of surface water with DIC, porewater (via tidal pumping), and alkalinity (Rosentreter et al., 2018a). Methanogenesis in the sediment leads to the production of CH_4 and controlled by soil redox (Zedler & Kercher, 2005). The production of CH_4 is dependent upon the availability of sulfate in the sediment and the salinity of the system (Ouyang

et al., 2017). CH_4 is emitted from the system at the sediment-water interface through pneumatophores, plant roots, and crab burrows (Rosentreter et al., 2018b). Salt marshes release more CH_4 from the sediment whereas mangrove release more CO_2 (Alongi, 2020a). The majority of N_2O production occurs from sediment denitrification, with the water column contributing a large amount of N_2O through nitrification in suspended particles (Murray et al., 2015). N_2O fluxes and controlled by levels of dissolved inorganic nitrogen (DIN) and oxygen availability in the system, which are affected by groundwater inputs, tidal cycles, and macrophyte density (Murray et al., 2015). Some mangrove species can function as a sink of N_2O (Macreadie et al., 2019), which can help mitigate the effects of climate change and sea-level rise.

1.5 Isotope Chronometers

By using paired radioisotopes of carbon and lead (^{14}C and ^{210}Pb) to ascertain the amount of primary production stored in peat, it is possible to study carbon transport through peat systems and examine first-order changes in carbon stock through time (Breithaupt et al., 2014; Breithaupt et al., 2020; Schafer, 2020). Due to its short half-life (22.3 years), ^{210}Pb is an effective tracer of sediment accumulation in shallow-water systems, where ^{210}Pb is supplied primarily from atmospheric fallout (Smoak et al., 2013). Establishing an independent ^{210}Pb chronology permits an interpretation of ^{14}C as a tracer of young atmospheric carbon in coastal wetland sediments (Schafer, 2020).

Thermonuclear weapons testing between 1955 and 1963 nearly doubled the amount of naturally occurring atmospheric ^{14}C in the Northern Hemisphere. This “bomb-derived radiocarbon” gradually diffused from the mid to high latitudes of the Northern Hemisphere to the lower latitudes and Southern Hemisphere (Trumbore, 2009) and was gradually incorporated into

carbon reservoirs in the ocean and biosphere (Trumbore, 2009; Schafer, 2020). Tree ring studies were used to compile initial profiles of bomb radiocarbon as a natural tracer and illustrate a large gradient in ^{14}C levels, leading to the distinction of four different atmospheric zones (Hua & Barbetti, 2004). Atmospheric ^{14}C levels peaked in 1963 in the Northern Hemisphere (Nydal & Lövseth, 1965; Kutschera, 2022), shortly after nuclear weapons testing ceased and has decreased exponentially since then. As a result, the bomb-derived radiocarbon record allows the inference of carbon exchange with the atmosphere in a reservoir on short timescales (Trumbore, 2009). The concentration of bomb ^{14}C in a soil sample can be used to calculate turnover times, giving insight into the flux of carbon between the soil and atmosphere (Trumbore, 2009).

1.6 Study Goals

In this study I will examine the efficiency of carbon sequestration through time in blue carbon ecosystems. I define efficiency as the ability of the system to retain carbon in burial instead of laterally outwelling. Previous research suggests that blue carbon ecosystems are efficient at carbon sequestration (Donato et al., 2011; Mcleod et al., 2011; Breithaupt et al., 2012; Alongi, 2014; Rosentreter et al., 2018b) but many lose a significant fraction of net primary production to coastal waters (Kristensen et al., 2008b). If most of the carbon is lost or recycled as a flux of atmospheric CO_2 (Chambers et al., 2013; Hansen & Nestlerode, 2014; Rosentreter et al., 2018b) or outwelled to the ocean, then the efficiency of the system must be questioned.

1.7 Research Questions and Hypotheses

To better understand the efficiency of blue carbon ecosystems, several questions must be addressed. For each question, I have proposed a testable hypothesis that will be considered in my

work. The first question builds upon the work of Schafer, 2020, where it was determined that bomb-derived carbon in mangrove sediments has a longer turnover time than that of the atmospheric bomb curve. When graphed, mangrove soils have a more elongated shape with a low peak, which is much different from that of the graphical profile of atmospheric bomb radiocarbon.

Q1: Is bomb-derived carbon preserved similarly in salt marsh and mangrove sediments?

H1: Salt marsh sediments will exhibit longer carbon turnover times like what is observed in mangroves and will have a low $\Delta^{14}C$ peak when graphed.

The work of Schafer (2020) examined the depth and concentrations of bomb-derived radiocarbon in mangrove sediments using ^{210}Pb as an independent chronometer and ^{14}C as an environmental tracer. It was determined that mangrove sediments show evidence of bomb-derived radiocarbon at depths representative of the 1800s, before atmospheric testing of thermonuclear weapons began (Fig. 3). Using these dual isotopes, soil turnover times were calculated and the carbon transport mechanism to depth in the sediment was studied. The carbon transport depth has not been studied in salt marsh sediments.

Q2: What insights can coupled ^{210}Pb and ^{14}C measurements provide for carbon transport to depth in salt marsh sediments?

H2: Coupling measurements of the radioisotopes ^{210}Pb and ^{14}C will allow the establishment of an age-depth relationship while also tracing younger carbon to depth in salt marsh sediments.

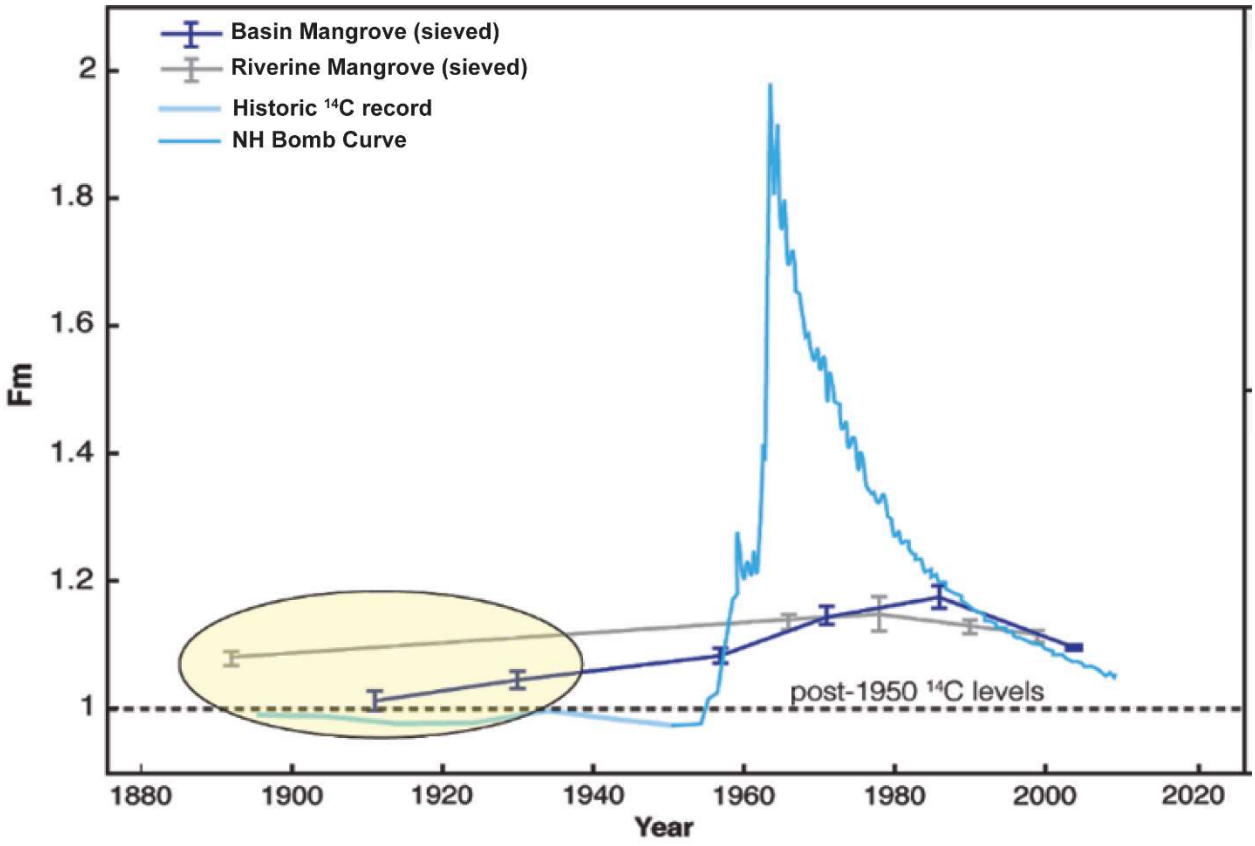

Figure 3. *^{14}C results from the riverine and basin mangrove sites, comparing the atmospheric bomb curve to ^{14}C values from both sites. The yellow circle indicates where intervals of post-depositional movement of carbon is apparent due to Fm > 1. Error bars are derived from blank correction and analytical error (Schafer, 2020).*

Effluxes from the system have been examined in several studies using methods such as discrete water sampling, laboratory incubations, and benthic flux chamber collections (Scudlark & Church, 1989; Kadlec, 2000; Murray et al., 2015; Rosentreter et al., 2018b). To date, it has not been determined if the efflux of DIC and CO_2 can be estimated using the influxes of carbon to the system. Due to the complicated nature of measuring efflux values, I aim to employ a model that will simplify the process and avoid certain errors by using the estimated influx values.

Q3: Can the efflux of DIC and CO_2 be estimated by using carbon influxes to the system?

H3: Differences between preserved sedimentary bomb ^{14}C concentrations and atmospheric bomb ^{14}C can be explained by efflux of DIC and CO_2 from the system, providing a measure of carbon burial efficiency.

CHAPTER TWO:

METHODS

2.1. Site Description

Peat cores were collected from the Charlotte Harbor (Gerlach et al., 2017) and Ten Thousand Islands (Schafer, 2020) regions of Southwest Florida (Table 2 & Fig. 4). Charlotte Harbor estuary is home to a robust mangrove and salt marsh community, including *Juncus roemerianus, Spartina alterniflora*, and *Spartina patens* (Taylor, 1974). The harbor is predominantly shallow (less than 1.83 m) and has a maximum tidal amplitude of 0.9 m, except when severe weather conditions occur (Taylor, 1974). Charlotte Harbor cores were taken from Long Island (Gerlach et al., 2017), where the Peace River enters Charlotte Harbor and the area of salt marsh is larger than the area of mangroves (Taylor, 1974; Beever III et al., 2012; Radabaugh et al., 2017).

Study sites in the Ten Thousand Islands serve as two different classifications of mangrove systems – riverine and basin. The riverine mangrove site is an overwash mangrove island (Schafer, 2020) located near the mouth of the Upper Faka Union Canal. Situated ~5 km from the Gulf of Mexico, this site is exposed to constant flushing from the daily tidal fluctuations and canal water flow. Basin mangrove cores were collected from Cat's Claw Basin, which is more isolated than a typical basin mangrove system due to an enhanced berm on the western edge of the forest (Radabaugh et al., 2019; Schafer, 2020). This site is situated between the berm and a raised road to the north, causing a reduction in tidal flow. The dominant vegetation at both sites is red

(*Rhizophora mangle*) and black (*Avicennia germinans*) mangroves with periodic white (*Laguncularia racemosa*) mangroves (Twilley, 1985; Schafer, 2020).

Table 2. *Salt marsh, riverine mangrove, and basin mangrove site information.*

Site	Location	GPS	Dominant species
Salt Marsh	Long Island, Charlotte Harbor	26° 57' 51.51" N, -82° 0' 2.82" W	*Juncus roemerianus*
Riverine Mangrove	Upper Faka Union Canal	25° 54' 6.70" N, -81° 30' 38.05" W	*Rhizophora mangle, Avicennia germinans*
Basin Mangrove	Cat's Claw Basin	26° 1' 18.23" N, -81° 44' 1.54" W	*Rhizophora mangle, Avicennia germinans*

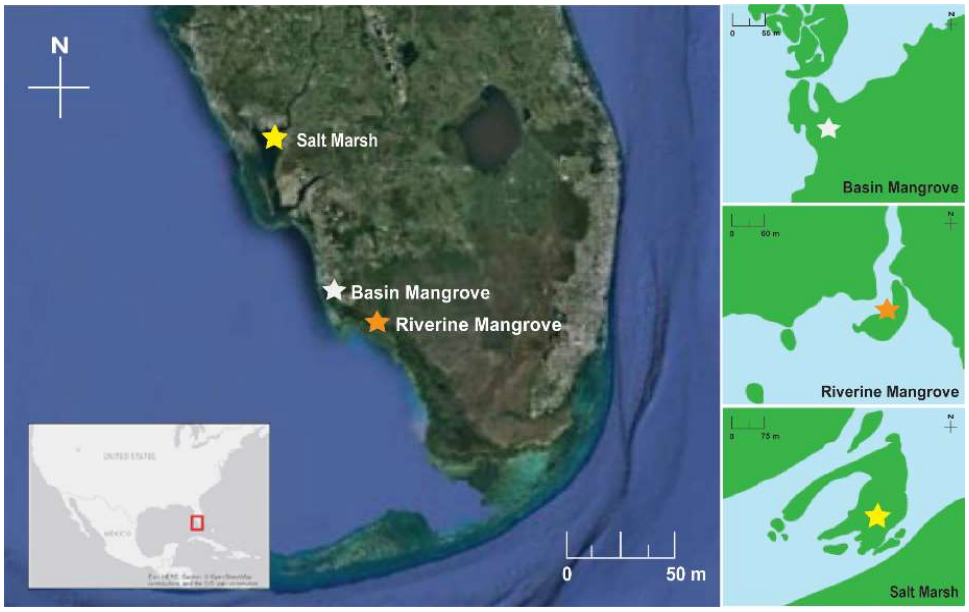

Figure 4. *Map of study sites in Charlotte Harbor and Ten Thousand Islands, Florida, U.S.A. The salt marsh and riverine mangrove sites are subject to near constant flushing from the surrounding canal. The basin mangrove site experiences a reduced tidal flushing regime. Adapted from Schafer (2020).*

2.2. Sample Collection

Two cores were collected at each site, a short push core (~25 cm) and a longer core (50-100 cm). The longer peat core was collected using a stainless steel half-barrel (D-type) peat corer

(Belokopytov & Beresnevich, 1955; Jowsey, 1966), which collects half of a core by rotating around the sediment sample that is to be collected. This coring method helps prevent contamination or compaction of the sediment during collection. The core was transferred to a polyvinylchloride (PVC) sleeve, wrapped in PVC film, and labeled accordingly. Cores were stored in a cooler in the field to minimize temperature variability and limit photooxidation until arrival in the laboratory.

2.3. Sample Filtering and Acid Treatment

Upon arrival at the laboratory, all cores were stored in a refrigerator at 4 °C until analyses could be completed to slow biological activity occurring within the sediment. In the laboratory, each long core was sampled at 1-cm intervals throughout the entire 50-cm core. Each sample was then weighed and labeled accordingly.

Samples were filtered and acid treated to remove any large particles, roots, and carbonates that may be present. Samples were mixed with 2000 mL of DI water and sieved through 500 and 63 μm mesh sieves. The slurry created from particles <63 μm was filtered through four weighed and pre-combusted (900 °C, 4 hours) quartz filters. The filtering apparatus was composed of a large Erlenmeyer flask topped with a post, glass frit and metal clamp (Schafer, 2020) (Fig. 5). Once ~500 mL of the slurry had been filtered, the filter was removed and put into an oven to dry for 24 hours at 53 °C. After all filters were completely dry, they were weighed, and the initial filter mass was subtracted to obtain dry sediment masses.

For acid treatment, the same filtering apparatus was used, and previously filtered samples were treated. Filters were submerged in 1M HCl for 30 minutes. If the acid filtered through, more was added until the sample was fully submerged. After 30 minutes, filters were rinsed with DI water until a pH of ~6 was achieved. Filters were then removed from the filtration apparatus and

dried in the oven for 24 hours at 53 °C. Filters were weighed after drying and that mass was subtracted from the initial filter and sample mass to determine the carbonate mass of the sample.

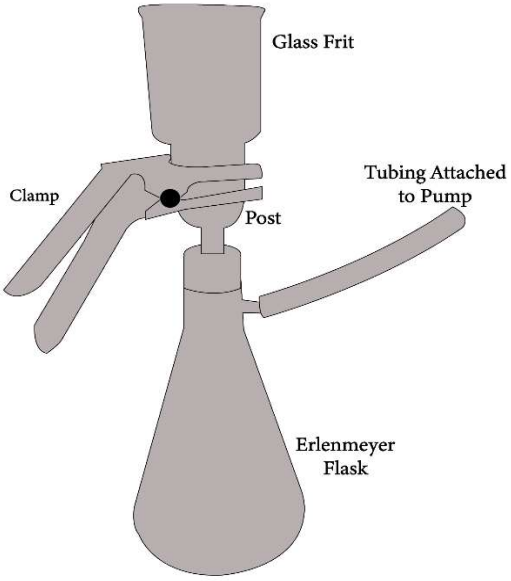

Figure 5. *A schematic of the filtration apparatus. Quartz filters are positioned between the post and glass frit and secured with the clamp (Schafer, 2020).*

2.4. Bulk Combustion

Dry sediment samples were pulled from filters using pre-combusted (525 °C, 4 hours) forceps. Salt marsh and mangrove sediments range from ~1-12% TOC (Bianchi et al., 2013) – for this study I assumed 6% TOC when weighing samples. Sediment pieces were weighed to obtain ~30 µmol of CO_2, which was determined stoichiometrically from the %TOC. Once the desired weight was reached, the sample was transferred to a pre-combusted (900 °C, 4 hours) quartz tube including 1 cm of silver wire and 150 mg of CuO. Quartz wool was inserted on top of the sample, to prevent escape, and the tube was connected to the vacuum line (Fig. 6) to remove atmosphere

and flame-seal for combustion. Sealed tubes were put into the muffle furnace to combust at 900 °C for 4 hours, converting all OM to CO_2.

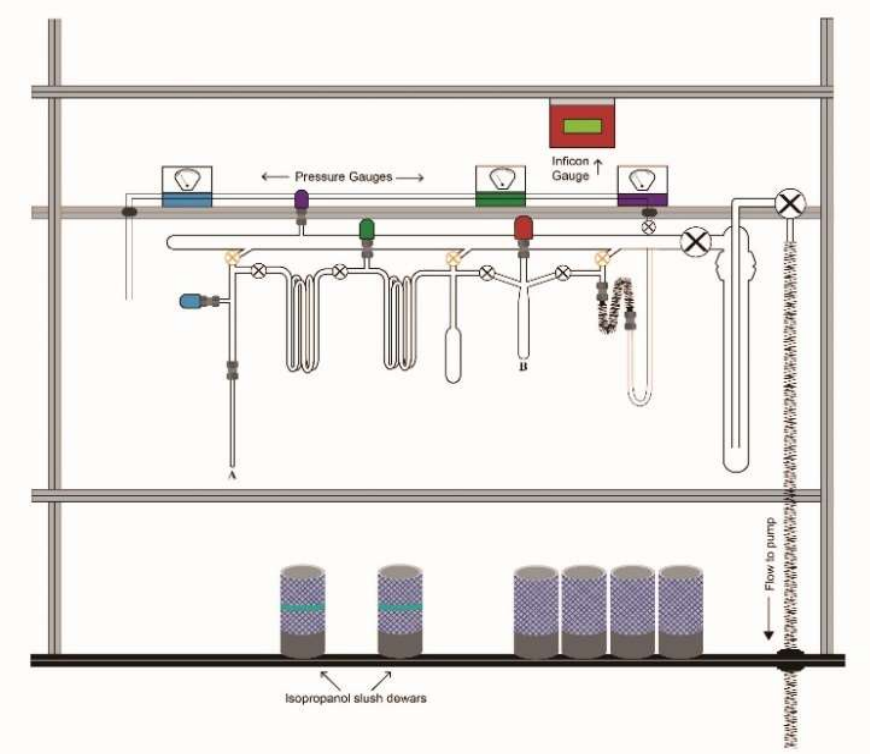

Figure 6. *Schematic of the vacuum line used for bulk combustion. Tubes are cracked at point A, cryogenically purified, and moved downstream to be quantified manometrically at point B, then moved back to point A for flame sealing (Diagram from T.M. King).*

Combusted samples were purified before radiocarbon dating. Tubes were reattached to the vacuum line and cracked to release the gaseous sample. Water vapor was removed using an isopropyl slush that was cooled to transition phase with the liquid nitrogen (-77 °C). Once the sample was purified the gas volume was manometrically quantified, the sample was resealed into a pre-combusted Pyrex tube (525 °C, 4 hours). All collected samples were sent to National Ocean Sciences Accelerator Mass Spectrometry (NOSAMS) facility for ^{14}C and $\delta^{13}C$ measurements.

2.5. Chronometers

Lead-210 was used as an independent chronometer whereas radiocarbon was used as a natural tracer. These radioisotopes were employed to constrain the limits of the chronology within the core, as well as determine accretion and exchange rates.

2.5.1 Lead-210

All push cores were ^{210}Pb-dated using methods initially described in Smoak et al. (2013). A constant rate of supply (CRS) model (Appleby & Oldfield, 1978) was used to determine the ^{210}Pb ages and mass accumulation rates of sediment within the system. This model is useful because it assumes variable sedimentation rate, with a constant supply of ^{210}Pb, over the course of the record. Profiles of downcore ^{210}Pb allow for the evaluation of the impact of bioturbation in the system (Table 4, Appendix A).

2.5.2 Radiocarbon (^{14}C)

The longer cores were to extend the ^{210}Pb chronology. Two preparation methods were used to obtain the ^{14}C content of the samples – Ramped Pyrox and bulk combustion techniques. Ramped Pyrox is a ^{14}C preparation method that separates soil organic matter based on thermochemical stability and allows the examination of a ^{14}C age spectrum within a sample (Rosenheim et al., 2008). Ramped PyrOx is a useful tool for measuring radiocarbon in samples from systems with multiple OC sources (Rosenheim et al., 2008), whereas bulk combustion is useful when there is one source of OC, or the ages of the OC are similar. In bulk combustion, the total sample is combusted at the same temperature, combining CO_2 from labile and refractory ^{14}C sources in the sample. Initial ramped PyrOx analyses (δ^{13}C and ^{14}C) of the mangrove sites indicated samples

were dominated by a single source of OC (Schafer, 2020). As a result, salt marsh samples were measured using gas produced by bulk combustion techniques only (Table 5, Appendix A).

2.6 Advection and Diffusion in Blue Carbon Systems

Carbon cycling within blue carbon sediment is unique due to its non-steady state, where mineralization, burial, and OC inputs oscillate with plant uptake, tides, and release/uptake via roots (Alongi, 2020b). The exchange of nutrients and dissolved OM between the water column and intertidal areas can occur through advective porewater leakage into the water column during low and ebb tide or diffusive fluxes over the sediment-water interface during tidal inundation (Bouillon et al., 2007). The movement of carbon within a blue carbon system can be determined using an advection-diffusion relationship:

$$\frac{\delta C}{\delta t} + \frac{\delta}{\delta x}(uC) = D\frac{\delta^2 C}{\delta x^2} + J \qquad \text{Eq. 1}$$

where C is the concentration of the solute, t is the time, D is the molecular diffusivity, u is the fluid velocity, and J is the *in situ* source/sink term.

Advective flows rapidly transport particles into and out of sediment (Santos et al., 2012), with the rate of migration dependent on the pressure gradient and sediment permeability of the system (Bouillon et al., 2007). Bulk advection of fluid within the system can occur laterally or vertically. Several advective and groundwater export pathways exist, allowing for carbon to move within the system (Alongi, 2020b). Porewater advection is thought to be important in blue carbon systems and can be calculated as:

$$\frac{\partial[C]}{\partial t} = -u_z \frac{\partial[C]}{\partial z}$$ Eq. 2

where z is the depth beneath the sediment-water interface. The presence of burrows in the system can increase the sediment permeability, thus increasing advective flux (Santos et al., 2012).

When newer carbon is taken into the system, it is transported to depth via biodiffusion and deep root turnover (Wang et al., 1996). Nutrients can diffuse out of the sediment and into the porewaters once deposited and circulate about the system via tidal pumping (Krom & Berner, 1980). To calculate diffusion, I used the equation:

$$\frac{\partial[C]}{\partial t} = D_z \frac{\partial^2[C]}{\partial z^2}$$ Eq. 3

where D_z is the vertical diffusivity coefficient for solute C. During transpiration, blue carbon vegetation excludes salt, which accumulates near the roots and must be transported away via diffusive processes (Hollins et al., 2000). If the salt diffuses into a macropore, such as a crab burrow, it will be removed via tidal flushing (Hollins et al., 2000).

The Péclet number is a ratio of the advective timescale to the diffusive timescale in a system and deals with the physical transport of materials along a gradient (Jenkins, 2003). The Péclet number is calculated as:

$$Pe = \frac{UL}{\kappa}$$ Eq. 4

where U is the velocity of the flow, L is the length, and κ is the turbulent diffusion coefficient. A Péclet number greater than 10 indicates the system is dominated by advection whereas a Péclet number less than 0.1 indicates diffusive control on the system (Bachand et al., 2014). A Péclet value of 1 indicates that the two processes are generally equal.

2.7. Comparative Numerical Simulations

Lead-210 dates and $\Delta^{14}C$ concentrations from previous work indicate that younger carbon is being transported to depth in mangrove soils (Schafer, 2020), but it is not understood if this occurs in salt marsh sediments as well. To better understand the mechanisms and dynamics of carbon sequestration in these ecosystems, a simplified advection model was constructed to visualize the differences in concentrations of OC at differing depths (https://github.com/trmartin1/MangroveandMarshModeling). To assess the magnitude of differences between ^{14}C and ^{210}Pb dates, the atmospheric bomb curve was used as the base of the model. Radiocarbon dates were chosen that roughly approximate the bomb curve within the system and used to quantify the differences in the atmospheric bomb curve and the bomb curve within the system. A third, padded data set comprised of ^{14}C values that were padded back to 1800 CE was used.

2.7.1 Building the model

To model the accumulation of peat in blue carbon ecosystems, I started from the bottom boundary layer and build up. The first deposited sediment block comes from net primary productivity of the mangrove or salt marsh grass (PP), with a certain amount of the OC lost through downward advection. I defined the proportion lost through advection as downward mixing

proportion *p(z),* which is a function of depth *z* because the model allows for distributions of these proportions in any form. At the boundary layer, this proportion does not get incorporated and is lost, as there is no peat below for it to build on. Southwest Florida and the Florida Keys have a Pleistocene topographic surface upon which a basal limestone sand or siliceous sand layer from the mid-Holocene formed (Dodd & Siemers, 1971). Peat began accumulating on top of these sediments almost immediately. The quantity of peat accumulated (m) and its isotope composition (δ) during initial deposition on the boundary layer and at surface depositional layers above the boundary layer can be defined as:

$$m_0 = PP_0 \times \big(1 - p(0)\big) \qquad \text{Eq. 5}$$

$$\delta_0 = \delta_{PP_0} \qquad \text{Eq. 6}$$

Any subsequent depositional layers mix proportions *p(z)* of new primary productivity downward into the layers below. The depth to which mixing can occur is a variable that is set within the model. The amount of accumulation (m), export (e), and isotope compositions (δ and δ_e) of depositional layers above the boundary layer ($z = 0$) and below the surface depositional layer ($i > 0$) can be formulated as:

$$m_{z,i} = m_{z,i-1} \times \big(1 - p(z)\big) + m_{z-1,i} \times p(z-1) \times (1 - \varepsilon_z) - m_{z-1,i} \times (1 - \varepsilon_z) \qquad \text{Eq. 7}$$

where i is the number of iterations occurring at each depth z and indicates the number of depth increments affected by down-mixing. The variable α_e is the fractionation factor for the transformation of solid OC into the dissolved form for export. Generally, I assumed that $\alpha_e = 1$

(i.e., no fractionation). Further, to make the model indicative of the naturally occurring processes in these systems, I used:

$$\delta_{e_{z,i}} = \alpha_e \delta_{\varepsilon_{z,i}} = \alpha_e \delta_{z,i} \quad \text{Eq. 8}$$

where the isotopic signature of all inputs must equal the isotopic signature of all outputs. The conservation of mass within the system must be maintained.

2.7.2 Testing model sensitivity

Sensitivity tests were run to test how the choice of method of downward carbon affects the proportion of carbon mixed down and the depth to which is it mixed. Sensitivity is a determination of how much a model output is affected by a change in inputs. Each sensitivity test changes one variable within the model to understand what must occur within the model to cause changes in the output. Both a square wave and Gaussian function for downward carbon transport were tested, with the goal of fitting the data to a padded data set representing the atmospheric ^{14}C bomb curve. The square wave function constantly mixes down 50% from the above sediment interval until a point is reached where no more diminishments can occur. If a square wave function is used for downward mixing, I used $p(z) = p$ to define the mixing depth. Conversely, the Gaussian function mixes down a diminishing percentage of the above interval as the model follows a normal distribution downcore eventually arriving at 0% mixed down.

2.7.3 System fluxes

The model allows the inclusion of influxes and effluxes to balance the system and gain an understanding of how mangrove and salt marsh systems may differ in carbon cycling and storage dynamics. To conceptually constrain the amount of outgoing carbon from either system, flux data for the system must be used to constrain the model. The influx of atmospheric CO_2, DOC, and POC into the system and the outwelling of DIC and CO_2 from the system are the focus of this model (Fig. 2). POC influx and CH_4 and N_2O efflux are considered negligible (Zedler & Kercher, 2005; Saintilan et al., 2013; Persico et al., 2017; Maher et al., 2018). In addition to the depth of the core, several constraints must be observed when building the model, including bioturbation, root depth, and tidal range. Crab burrows extend up to 1 m into the soil (Martinetto et al., 2016). The average root depth is 40 cm in salt marshes (Redelstein et al., 2018) and 1-2 m in mangrove soils (McKee et al., 2007).

2.7.4 Carbon export

Because the system cannot export more than it takes in without causing a collapse of the system, this balance of mass must be considered. The export term (ε) was used for lateral and downward export, as both occur in blue carbon ecosystems. I considered lateral export at two different instances in the model. When leaf litter is deposited, lateral export occurs from the system before the litter can decay (Twilley, 1985). Tides can carry the leaf litter from where it is produced, meaning it will not get incorporated into the sediment. If the litter is deposited, it can laterally outwell from the system in the form of DOC and POC after decomposition, typically aided by porewater exchange (Alongi, 2020b). Both forms of export are important to the functioning of the system, therefore both must be incorporated into the model. Lateral export was calculated as:

$$e_{x,i} = m_{z,i-1} \times p(z_i) \times \varepsilon_{z,i}$$ Eq. 9

After deposition in the system, byproducts of primary production are broken down by microbial activity and become DOC and POC within the soil. This OC is exported downward through the soil and aids in belowground primary production (Alongi, 2020b). I calculated this downward export as:

$$e_{z,i} = m_{z,i-1} \times p(z_i) \times (1 - \varepsilon_z)$$ Eq. 10

$$\delta_{z,i} = \frac{m_{z,i-1} - e_i}{m_{z,i}} \times \delta_{z,i-1} + \frac{e_i}{m_{z,i}} \times \delta_{z-1,i}$$ Eq. 11

The horizontal advection coefficient $\varepsilon_{z,i}$ can be used to assign advection out of the model as an overall export function. The export can be held constant or vary with time based on independent constraints. This factor allows us to estimate the amount of carbon that leaves the system, so that the model can approach the observed trends in downcore carbon isotope composition.

CHAPTER THREE:

RESULTS

Lead-210 dates from all samples were compiled and rounded to the nearest year (Table 4, Appendix A). These dates were coupled with the ^{14}C concentrations for the upper soil strata to examine carbon movement post-deposition. Given that there is an exponential decline in excess ^{210}Pb within the sediment, I know that ^{210}Pb did not migrate after deposition, thus establishing an age-depth relationship for building the model. Within the top 25 cm of the core, the ^{210}Pb chronology extends to different age maxima, with the salt marsh system reaching 1937 CE, the riverine mangrove system reaching 1892 CE, and the basin mangrove system reaching 1911 CE. Initial isotopic measurements ($\delta^{13}C$ and ^{14}C) of the mangrove soils indicated samples were dominated by a single source of OC (Schafer, 2020). As a result, salt marsh samples were dated using bulk combustion techniques only. All fraction modern (Fm) values denote modern deposition (Table 5, Appendix A). The $\delta^{13}C$ value of the samples ranged from -29.97 to -25.06 ‰, indicative of terrestrial origin and the dominance of C3 vegetation in all samples (Tables 5-6, Appendix A). Average accretion rates were higher in the basin mangrove system (2.51 mm y^{-1}) than in the riverine mangrove (2.40 mm y^{-1}) or salt marsh system (1.30 mm y^{-1}).

The calculated Péclet number for salt marsh and mangrove systems is 1.26 in mangroves and 149.25 for salt marshes (Kristensen et al., 2011; Leopold et al., 2015; Santos et al., 2019; Xiao et al., 2021). This indicates that advection is 1.26 times more important in the mangrove system than diffusion and nearly 150 times more important in the salt marsh system. Because the Péclet

number is greater than one in both systems, diffusion was not considered in the building of the model.

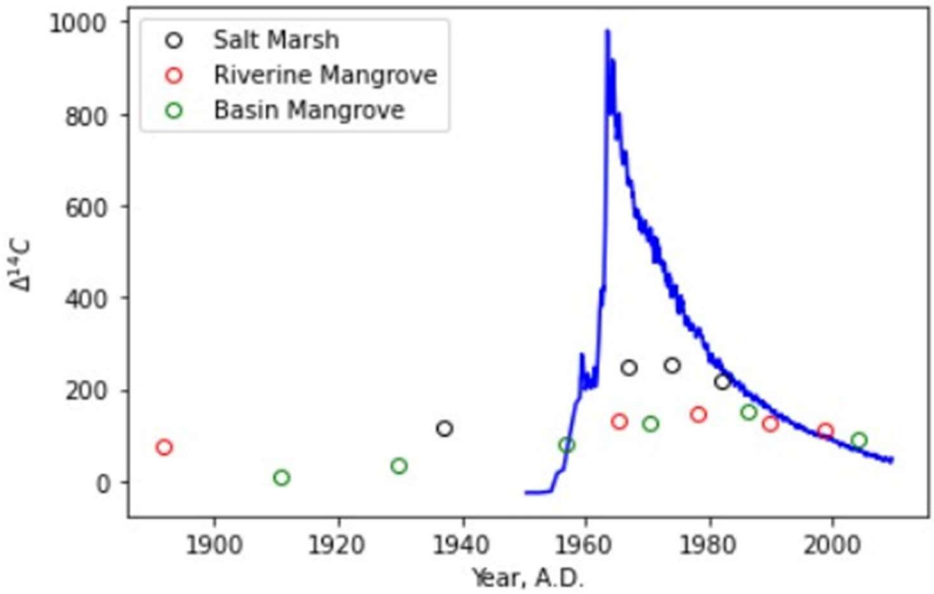

Figure 7. *The Northern Hemisphere radiocarbon bomb curve (blue line) compared to the data collected for salt marsh, riverine mangrove, and basin mangrove sites. All exhibit elongated shapes with no defined peak, suggesting longer carbon turnover times.*

The atmospheric bomb curve shows a sharp increase in atmospheric ^{14}C concentrations that peaks in the early 1960s and steadily declines thereafter (Fig. 7). Instead of this sharp peak, each site showed a smoother, more elongated curve with no discernible peak – indicating that there are longer turnover times for younger carbon within the soil. To further compare the data from this study to the bomb curve, a padded data set was used to directly examine dates before bomb testing. This data set was comprised of ^{14}C values that were padded back to 1800 CE because the age constraints on the data in this study extend to 1892 CE. Because there is no direct measurement of atmospheric ^{14}C prior to the 1940s, data from the calibration curve must be used to directly compare the data from this study to the bomb curve. Results of this test were similar, with a more

elongated curve seen in the study data than was seen in the padded data. Salt marsh data showed a higher ^{14}C peak than the mangrove data sets.

Model variables were evaluated using a range of values for each system, with the goal of determining the best fit of the model to the data. Sensitivity tests conducted for each system resulted in no significant difference between the functional form of mixing employed, indicating that the model is not sensitive to the method of downward transport. The model is slightly more sensitive to the square wave function, with the amount of carbon moved down from each sediment interval fitting closer to the study data. Carbon mixing depth was examined for each system, which was defined as the number of increments over which the signal propagates (Fig. 8). The basin mangrove system had a deeper mixing depth (Table 3) than the salt marsh or riverine mangrove system. At a mixing depth equivalent to 100 years, the model began converging together into a single point, indicating that the model could only manage data to a certain age. Values obtained from the mixing depth runs were used to find the maximum proportion of material that is mixed down into the sediment block immediately below the block that was just deposited. The basin mangrove system had the largest proportion of carbon mixed down, whereas the salt marsh and riverine mangrove systems had much smaller proportions of carbon mixed down between increments (Fig. 9). Carbon is continually exported from the system, both before and after deposition into the sediment column. To account for this, a carbon export term was added to the model. The salt marsh system shows the largest amount of carbon export from the system whereas the mangrove systems export less carbon (Fig. 10). Although I obtained optimal variable values for each system, I was not able to fit the model to the data sets.

Table 3. *Model outputs for all systems. Mixing depth is defined as the number of increments over which the signal propagates. Mixing proportion is the maximum amount of material mixed down into the increment below. Carbon export accounts for export from the system before and after deposition into the sediment column.*

System	Mixing Depth (yrs)	Mixing Proportion	Carbon Export
Salt Marsh	25	0.2	0.6
Riverine Mangrove	75	0.3	0.5
Basin Mangrove	120	0.5	0.545

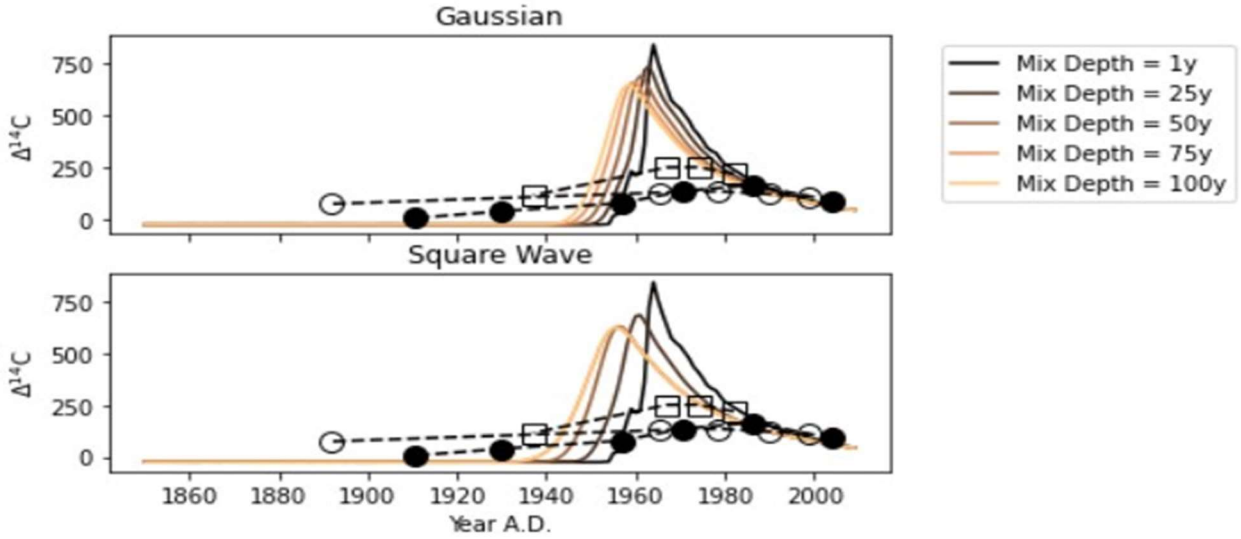

Figure 8. *Model output for mixing depth using Gaussian and square wave functions. The black line is a close estimation to the radiocarbon bomb curve, and the different systems are indicated by the shapes with dashed lines. The salt marsh system is indicated by the squares, whereas the mangrove systems are indicated by the circles. The open circles are for the riverine mangrove system and closed circles are for the basin mangrove system. The basin mangrove system had a deeper mixing depth (120 years) than the salt marsh or riverine mangrove system (25 and 75 years, respectively).*

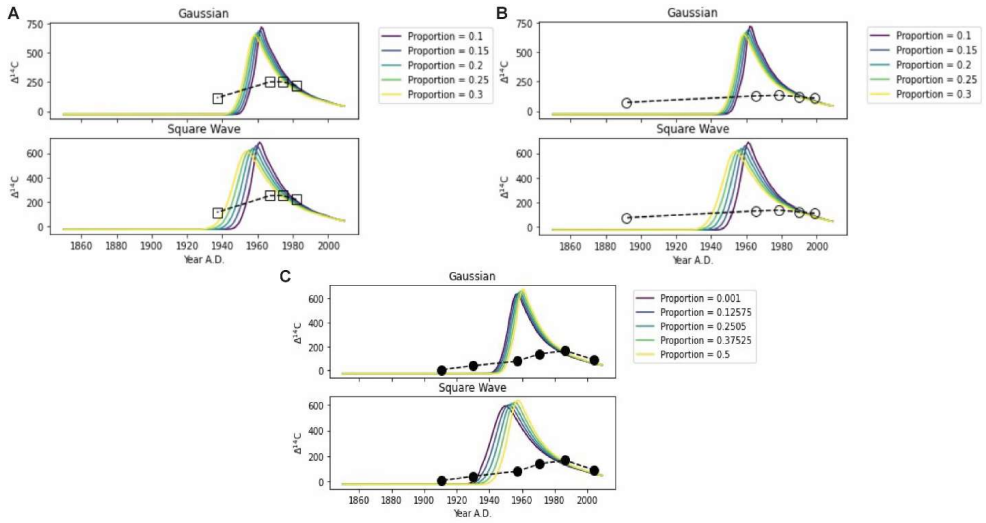

Figure 9. *Model output for proportion of material mixed down from the overlying sediment block. All systems had proportions less than or equal to 0.5 mixed down. A) The salt marsh system has a the smallest (0.2) mixing proportion. B) The riverine mangrove system has a 0.3 mixing proportion. C) The basin mangrove system had the largest proportion of carbon mixed down (0.5).*

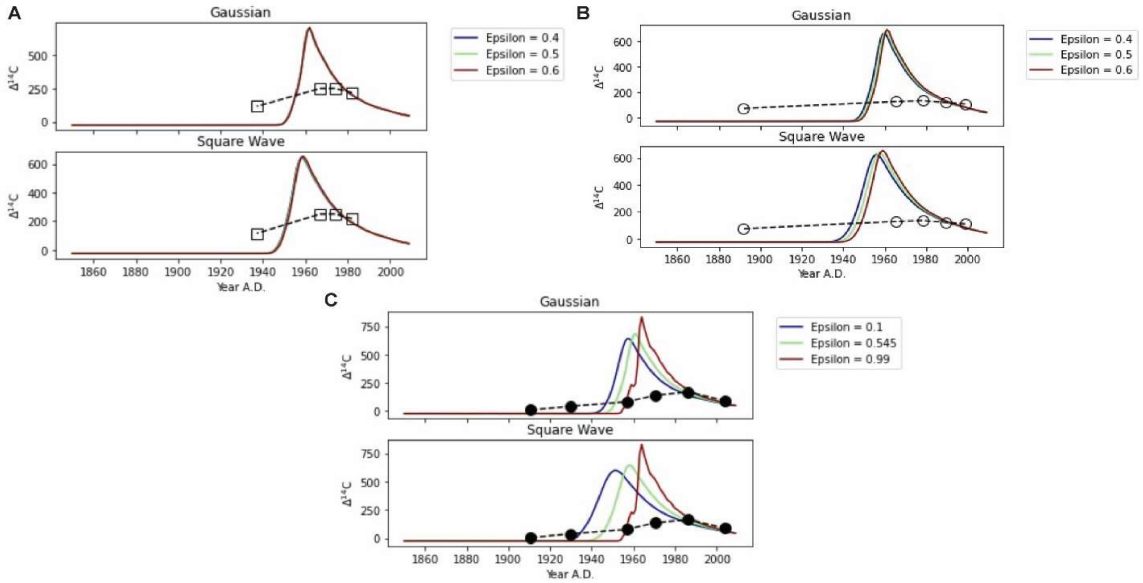

Figure 10. *Model outputs for carbon export in the A) salt marsh system, B) riverine mangrove system, and C) basin mangrove system. The salt marsh system shows the largest amount of carbon export from the system (0.6) whereas the mangrove systems export less carbon (0.5 in riverine and 0.545 in basin systems).*

CHAPTER FOUR:

DISCUSSION

4.1 Carbon transport to depth

Younger carbon is transported to depth within the sediment column of blue carbon ecosystems. Microbial activity, root exudates, and bioturbation aid in the transport of this labile carbon. Bioturbation, aided by tidally-driven advection, is integral in the downward transport of carbon and has been shown to have a large effect on the biogeochemical processes occurring in blue carbon ecosystem soils (Koretsky et al., 2002; Kristensen et al., 2008b; Martinetto et al., 2016). Burrows increase the surface area available for biogeochemical exchange at the sediment-water interface, allowing for higher rates of advection to occur due to increased soil permeability (Bouillon et al., 2007; Santos et al., 2021). As bioturbating organisms move older material out of the burrow and deposit fresh detrital material along the burrow (Kristensen et al., 2008b), large quantities of remineralized nutrients are accumulated and concentrated in the water within the burrows (Martinetto et al., 2016). This expedites the decomposition of OM and provision of newer OC at deeper depths. Remineralized nutrients and metabolic products are delivered to the sediment-water interface via porewater exchange or tidal pumping (Reithmaier et al., 2020) whereas newer carbon is transported to depth through vertical biodiffusion and deep root turnover (Wang et al., 1996). The existence of younger carbon at depth in this study supports the notion that crabs and other bioturbating organisms are responsible for transporting younger carbon into the sediment column. Results from the model indicate that square wave function, which lends support to the notion that bioturbation is an important transport mechanism.

Blue carbon ecosystems are driven by pore- and groundwater advection (Maher et al., 2013; Alongi, 2020b; Santos et al., 2021). The existence of extensive networks of roots and burrows, coupled with high porewater flow to assist in advective processes, lends to the support of the high Péclet number in each system. These macropores improve soil aeration and provide an efficient mechanism for the advective or diffusive removal of excess salt in the root zone (Xiao et al., 2019). There is thought to be a continual advective porewater exchange with crab burrows and the surrounding soil (Xiao et al., 2021). Some research suggests that nearly all respired carbon within the system is released in the dissolved phase through advective porewater exchange or lateral transport to adjacent tidal waters (Alongi, 2020b). Substantial portions of the DIC and DOC exports in blue carbon systems are driven by advection porewater exchange (Bouillon et al., 2007; Maher et al., 2013; Santos et al., 2019). Biogeochemical compound transportation via advective flushing can be orders of magnitude higher than molecular diffusion (Santos et al., 2012; Santos et al., 2021). That said, it is possible I should have included diffusion in the model. The Péclet number of salt marshes supported the use of an advection only model for this study. However, the calculated Péclet number in the mangrove system shows that advection is only slightly more important than diffusion, which could mean that this system would benefit from an advection-diffusion model. Perhaps, use of such a model could have resolved the ill fit of the model to study data.

4.2 Coupling ^{210}Pb and ^{14}C

Lead-210 gives the sedimentation rate and time parameters in the model and provides a chronometer that is free from the influence of any biological processes that occur within the system. There is a constant supply of ^{210}Pb from the atmosphere, which does not get taken into

vegetation or roots but is instead mixed down through the sediment. There will be a maximum amount of ^{210}Pb in the top layers of sediment, but the quantity present will decrease with depth and eventually disappear. Thus, measuring ^{210}Pb levels within the soil will give an independent time measurement of the age of the soil. When ^{210}Pb is coupled with ^{14}C as a natural tracer, insight into carbon cycling within the sediment can be gained. Radiocarbon has a much longer half-life (5,730 years) than ^{210}Pb (22.3 years) and is incorporated into the vegetation and roots of the system. As a result, bomb-derived ^{14}C is distributed throughout the soil via the root system and microbial mixing. Newer carbon inputs to the system should be diluted by older carbon in the soil. Bioturbation, including burrowing fauna and roots, disperses the carbon throughout the sediment column and provides a method for mixing newer carbon into the system.

By coupling ^{210}Pb and ^{14}C, I was able to determine an age-depth relationship while also tracing the movement of younger carbon from the surface to depth downcore. The riverine and basin mangrove systems have older measured ^{210}Pb ages (1892 CE and 1911 CE, respectively; Tables 6-7, Appendix A) than the salt marsh system (1937 CE; Table 5, Appendix A). However, because I do not have ^{210}Pb dates for the two lowest intervals of sediment in the salt marsh system, it is possible that the chronology would extend to an older date than what I observed in the mangrove systems. Bomb-derived radiocarbon is preserved in both mangrove and salt marsh systems (Fig. 7) though it appears to be preserved at greater depth in mangrove systems (Fig. 8).

4.3 Carbon sequestration

Blue carbon ecosystems sequester CO_2 from the atmosphere and fix it into OC that is used for primary production. Organic carbon is shed from the plant, often in the form of litter, and enters the soil to be decomposed and microbially altered. Previous research has demonstrated that carbon

is exported from the systems to the coastal ocean as DOC, DIC, or POC. When compared, DOC is exported in a larger amount than POC (Twilley et al., 1992), but DIC makes the largest contribution to carbon export from the system to the coastal ocean (Maher et al., 2013; Alongi, 2014; Ouyang et al., 2017; Reithmaier et al., 2020; Alongi, 2020a; Cabral et al., 2021; Santos et al., 2021). Whereas export to adjacent waters is often ~40% of carbon from net primary production (Duarte, 2017; Twilley et al., 2017), results from this study indicate that 50-60% of the carbon produced is exported from the system. The definition of DIC export varies between studies, with some using a combination of DIC, CO_2, and CH_4 (Alongi, 2014; Ouyang et al., 2017), some studies combining DIC and CO_2, but separating CH_4 (Alongi, 2020a), and some studies separating all inorganic carbon terms (Santos et al., 2019). In the model, I assumed all carbon exported from the system was in the form of DIC, with no distinction for speciation. Future work will need to examine the carbon speciation, to gain a better understanding of which forms of carbon are exported from the system.

Blue carbon soils are generally a net source of CO_2 and CH_4 to the atmosphere (Alongi, 2005), which acts as an offset to burial and long-term storage (Maher et al., 2018). Salinity and sulfate availability affects whether CO_2 or CH_4 gas is released from the sediment (Rosentreter et al., 2018b). Methane is released via diffusion of plant tissues, bubble formation, and water diffusion within the system (Zedler & Kercher, 2005). The emission of CH_4 from blue carbon systems is variable but is often enhanced by the presence of pneumatophores and plant roots (Rosentreter et al., 2018b). Whereas salt marsh sediments release more CH_4 and export more dissolved CH_4, mangrove soils release more CO_2 and export greater amounts of POC, DOC, and DIC to coastal waters (Alongi, 2020a). This CO_2 efflux from sediments and tidal export of DIC appear to be the major sinks to the coastal ocean (Bouillon et al., 2008). Sediment metabolic

activity and efficient exchange between porewater and surface water has been credited for the high CO_2 flux rates from mangrove waters (Rosentreter et al., 2018a). According to Pendleton (2012), >97% of soil OC losses are from microbial respiration, which fluxes CO_2 back to the atmosphere. The level of outwelled CO_2 (Santos et al., 2019), DIC (Santos et al., 2021), and CH_4 (Zedler & Kercher, 2005) is large in blue carbon ecosystems.

Research suggests that salt marshes have the highest carbon sequestration ability but a lower carbon budget due to a limited and declining global extent (Ouyang & Lee, 2013). Carbon sequestration within the top meter of soil averages 0.02 Tg C km^{-2} in salt marshes (Alongi, 2014, 2020a) and 0.03 Tg C km^{-2} in mangrove soils (Alongi, 2014, 2020a). As mangrove encroachment into salt marsh systems slowly occurs, carbon sequestration and stocks change, often with the sequestration capacity of the mangroves increasing (Kelleway et al., 2016; Steinmuller et al., 2020). This is most likely due to the higher ability of the salt marsh soils to store carbon, which is attributed to the reduced mineralization rate, constant deposition of allochthonous sediment, and the coupled high primary productivity and low export rates that allow organic matter accumulation (Ouyang & Lee, 2013). Salt marsh sediments in this study had a high export value, which could be attributed to the location in Charlotte Harbor. According to local tide gauge info (NOAA #8725541), the Peace River has a tidal range of 0.07-0.59 m, which subjects the Long Island site to frequent inundation. This inundation allows the movement and export of carbon from the system. In addition to tidal influence, the riverine location of this site also allows for the site to benefit from discharge of carbon from upstream.

4.4 DIC export

The export of DIC is a substantial, but largely unaccounted for, blue carbon sink (Maher et al., 2013; Ho et al., 2017; Maher et al., 2018; Santos et al., 2019; Reithmaier et al., 2021). The budget for blue carbon systems is often unresolved or left with "missing" carbon (Bouillon et al., 2008; Alongi, 2009; Maher et al., 2013). It is possible that lateral export of DIC and OC mineralization within the soil contribute to the "missing" carbon in the budget (Chen et al., 2012; Maher et al., 2013; Leopold et al., 2015; Lovelock et al., 2015; Ouyang et al., 2017). There is often a high loss of carbon via outwelling that must be balanced to have a complete budget (Ray et al., 2018). It is likely that missing carbon sink is related to pore water-derived inorganic carbon fluxes (Chen et al., 2021) or DIC export from the system (Maher et al., 2013). Recent research has focused on the outwelling of DIC to balance the budget (Maher et al., 2018; Reithmaier et al., 2020; Santos et al., 2021).

Tidal activity plays a key role in litter dynamics within mangrove systems. Greater tidal activity and water turnover lead to higher litterfall and export of surface litter (Twilley et al., 1986) whereas decreased tidal activity would lead to greater *in situ* litter decomposition due to decreased export. When tides rise, water flushes the system and the newer OC is redistributed, causing a lateral transport of carbon throughout the system. The tide will also advance efflux from the system. In this study, the riverine mangrove system experiences greater tidal activity and a relatively high export of carbon from the system. The basin mangrove system, however, experiences a higher export of material than it should, given previous research. Tidal inundation only occasionally occurs in basin mangrove systems (Ewel et al., 1998). Carbon export from basin mangrove systems is dependent upon the amount of volume of tidal water inundating the system monthly and is responsive to seasonal increases in rainfall (Twilley, 1988; Twilley et al., 1992).

Given the high export value in the model, it is possible that the basin mangrove cores in this study were taken from an area that is frequently inundated. Rainfall events have also been shown to increase organic carbon export from mangrove systems (Twilley, 1985; Twilley et al., 1986). Cores for this study were taken in May 2017, which saw a higher amount of precipitation than is historically normal (https://www.weather.gov/wrh/Climate?wfo=mfl). Specifically, a week before cores were taken, the area experienced rainfall of 4 cm, which could have caused a high export of carbon from the area.

Mangroves have greater rates of subsurface DIC production (Alongi, 2020a) than salt marshes, which could help explain why the export values are so high in the basin mangrove system of this study. If more DIC is being produced, even if the area is not flooded as frequently, there may be more carbon exported when the inundation occurs. Root decomposition adds to the belowground carbon pool, which can, in turn, be exported from the system with the tide. Using my model, I examined export at two different steps in the process – before and after deposition into the sediment column – but there was not a substantial difference in the export value.

4.5 Model outputs

The objective of building this advective model was to distinguish how salt marsh and mangrove carbon cycling occurs, constrain the fluxes that have the most dominance in the system, and observe the depth to which a concentration of bomb radiocarbon can be detected. The model allows inclusion of in- and effluxes to balance the system and gain an understanding of how each system may be different regarding carbon cycling and storage. The difference in model outputs between the systems make sense when considering the differences in the vegetation in each area. The salt marsh system has a smaller mixing depth, smaller proportion of carbon mixed down

between layers, and a larger export value than the mangrove systems. Charlotte Harbor is a riverine setting, subject to frequent flushing from the surrounding water. The total biomass is less for the marsh than for the mangroves, but this system is subject to inputs of laterally exported carbon from the tides. Salt marsh grasses experience a more frequent turnover of standing biomass, with *Juncus roemerianus* having a turnover time of one to three years (Kruczynski et al., 1978; Stout, 1978). Salt marsh soils typically have quicker turnover times and roots that decompose more quickly than mangrove roots, which allows the input of younger carbon more frequently into the system (Alongi, 2020a). The mixing depth for this system was 25 years, which is within the constraints from previous studies (Redelstein et al., 2018).

Mangrove systems are subject to a large amount of autochthonous input, with some allochthonous inputs. Depending on the system there may be a flushing of fresh allochthonous material periodically, but not as frequently as in the salt marsh system. The riverine mangrove system is subject to more frequent flushing, like the salt marsh system. The berm near the basin mangrove system in this study limits the amount of allochthonous material that can be introduced to that system, except what may be deposited during a large storm or king tide event. In a basin mangrove system, OM contributes more to the formation of peat because the system is subject to less tidal inundation and leaf export (Twilley et al., 1986). This can lead to a thicker peat deposit than is seen in the other mangrove systems. Carbon concentrations in surface sediments of basin mangroves are typically higher and have lower turnover rates as a result of the thicker peat deposits (Twilley et al., 1986). In contrast, riverine mangroves experience increased litter export and decreased leaf decomposition *in situ* as a result of increased tidal inundation (Twilley et al., 1986). Observations like these align with the model outputs for the two mangrove systems. The riverine mangrove system has a higher mixing depth than the salt marsh system, but lower than the basin

mangrove system. The basin mangrove system also has the highest proportion of carbon mixed down between sediment blocks of any of the systems. Live roots are within the top 40 cm of soil (Alongi, 2012) but both mangrove systems had a mixing depth greater than this. Given that, it is likely that the mangrove systems are pulling carbon from the dead root pool in the sediment.

4.6 Modeling system efficiency

Blue carbon ecosystems are regarded as efficient in carbon sequestration. Due to the regular flooding and draining dynamics of blue carbon systems, material exchange to adjacent waters can be very efficient (Kristensen et al., 2008b). Blue carbon systems are very efficient at trapping suspended matter and organic carbon during tidal inundation periods (Mcleod et al., 2011; Subt et al., 2017). Because blue carbon systems can sequester allochthonous and autochthonous carbon, they are generally regarded as highly efficient carbon sinks (Chmura et al., 2003; Duarte et al., 2005; Bouillon et al., 2008; Lo Iacono et al., 2008; Duarte et al., 2010; Mcleod et al., 2011). High productivity and low sediment respiration lead blue carbon systems to be considered highly efficient in the sequestration of carbon into plant biomass and sediments (Jennerjahn & Ittekkot, 2002).

Despite the classification as efficient OC reservoirs, blue carbon systems can become net emitters of CO_2 to the atmosphere depending on the organic and inorganic carbon dynamics within the system (Mcleod et al., 2011). Whereas the budget is well-constrained in mangroves, uncertainties exist due to the poorly constrained mineralization pathways in the soil that are linked to CO_2 efflux (Macreadie et al., 2019). It has also been shown that 73% of the carbon from mangrove litter is respired and emitted as CO_2 into the atmosphere (Ray et al., 2018). Recent research has shown that there is a high level of outwelling to the coastal ocean (Santos et al., 2021).

Whereas this lateral outwelling accounts for less than 3% OC loss from the system (Alongi, 2012; Chambers et al., 2013; Martinetto et al., 2016; Santos et al., 2021), it must be considered when assessing the efficiency of blue carbon systems (Santos et al., 2021).

Initial runs of the model did not show any reactive loss from the sediment. Instead, the model served as a completely efficient endmember whereby 100% of the carbon going into the system stayed in the system. However, this completely efficient model is not realistic. It has been shown that blue carbon ecosystems are not completely efficient in nature (Twilley, 1985; Bouillon et al., 2008; Najjar et al., 2018; Macreadie et al., 2019; Alongi, 2020b; Santos et al., 2021). The inefficiency of blue carbon systems was demonstrated through use of the model. I was unable to fit the collected data sets to the atmospheric bomb curve, even after a reactive loss term was added. If I could have fitted the data sets, that would mean that the systems are efficient in storing carbon. Since I could not, the idea that blue carbon ecosystems are inefficient is supported.

The model does not force steady state but is constructed such that it should result in mass conservation, which can then be used to determine how the isotopic signature of the sediment may change. The input to the model is constant, using the average primary production of salt marsh and mangroves in Southwest Florida, and results in differing outputs for each system. As it is built, the burial efficiency should be determined based on what's left after processing. The lateral diffusion term in the model is net neutral, meaning I did not consider lateral inputs to the model. If the model forced steady state, the inputs would equal the outputs and mass conservation should occur. To attain mass conservation, it may be necessary to establish a horizontal gradient as a knob in the model that can be changed between runs. It could be that this horizontal gradient is the missing piece to making the model perfectly fit the data.

Carbon stored in the sediment is calculated by subtracting what has been exported from what was initially deposited, to gain a value of the amount of carbon that is left in the sediment column. There is a lateral carbon export through the system of leaf litter and wood before it can be deposited into the sediment column (Twilley, 1985), thus it will not be included in the carbon that goes into the sediment. After this point, I assumed that what is exported from the system is exported in the form of DIC and will result in the loss of some mass in the system. The calculated export of DIC from blue carbon systems is larger than other flux terms (Fig. 2) so I am confident in this choice. This is not to say that other forms of carbon cannot be exported from the system (DOC, POC, CO_2, or CH_4) as well. I simply do not control for these other forms of carbon in the model.

Annual primary production within the blue carbon ecosystem moves downward within the sediment and accumulates. If the system is completely efficient there would be annual carbon input plus the carbon input that is already present within the sediment, but there would be no loss of carbon. If this is true, there would be a constant concentration of carbon throughout the sediment and an extremely high concentration once the sediment boundary is reached. This is, however, not the case. As carbon goes through the sediment, it is subject to several reactions (e.g., DIC production or microbial respiration) that cause a loss of some amount of carbon from the sediment column.

Carbon storage and export results from this study are the opposite of what has been recorded in the literature. Typically, basin mangrove systems store more carbon than riverine systems due to the lack of export from the system. My results show that the amount of carbon stored in the basin mangrove system (80.11 Mg C ha^{-1}) was an order of magnitude lower than the riverine system (691.75 Mg C ha^{-1}). Assuming the cores taken are indicative of the system, riverine

mangroves in the Ten Thousand Islands store 5.04 x 10^6 Mg of carbon in the soil (Table 8, Appendix A). Making the same assumption, the amount of carbon stored in the Ten Thousand Islands basin mangrove system is an order of magnitude lower at 5.83 x 10^5 Mg. These results contradict that of Twilley et al., (1992), which showed that basin mangrove systems have a higher organic matter accumulation due to reduced export.

Peats in the Ten Thousand Islands have been dated at 3,500 years (Parkinson, 1989). During the time since peats have been forming in the Ten Thousand Islands, there has been 4.89 x 10^8 Mg C produced (Table 8, Appendix A). Peat in Charlotte Harbor have been dated to 2,180 years (Gerlach et al., 2017). During this time, 2.31 x 10^8 Mg C has been produced. When I compared these values to the amount of carbon stored in peat in Southwest Florida, the inefficiency of blue carbon systems was evident. The riverine mangrove system stored the largest amount of carbon (5.04 x 10^6 Mg C) whereas the basin mangrove system stored the least amount of carbon (5.83 x 10^5 Mg C). Salt marshes in Charlotte Harbor store 59.03 Mg C ha^{-1} and have a total carbon storage of 3.55 x 10^5 Mg of carbon in the sediment, assuming the cores taken are indicative of the entire system. When I compared the amount of carbon produced to the amount of carbon stored, the percent of carbon stored is exceedingly small (<1.05%) for all systems. Though some carbon is buried in the system, more is exported from the system than is stored, indicating that the system is inefficient.

The model allows for an estimate of export and transport that must need to happen to fit the bomb curve to the study data. Given that I could not make the model fit the study data, no matter how the variables were stretched or how unrealistically they were pushed, there must be missing information from the model that needs to be considered. Because I was unable to fit the model to the data, I can only provide an underestimation of export from the system. I did not

account for carbon export speciation in the model, meaning that I cannot know if the carbon leaving the system left in the form of dissolved carbon or was offgassed. A change like this well help examine if my export values are close to established literature values. The model did not account for a horizontal gradient that exists in blue carbon systems, thereby establishing mass conservation. Adding this piece would help to understand how the speciation of carbon changes as it travels through the system. Future work should also allow for quantification of carbon loss compared to carbon storage.

In my study, I defined efficiency as the ability of the system to retain carbon through burial instead of laterally outwelling it. Given this definition and the results from this study, blue carbon ecosystems are inefficient at sequestering carbon. My results indicate that a substantial portion of the carbon in the system is lost or exported as DIC. Instead of being efficient with carbon sequestration, I propose that blue carbon ecosystems are, instead, effective. Blue carbon systems are effective in sequestering CO_2 from that atmosphere, but not efficient in burying it in long-term storage. All three systems showed a large export of carbon ($\leq 50\%$) from the system, meaning that there would be less to be buried. I did not tabulate the burial of carbon using the model, but if I know that more than 50% of the carbon produced is being exported, that does not fit my definition of efficiency. Additionally, given that the amount of carbon stored in the blue carbon systems of this study is less than 1.05% for all systems, I must assert that the carbon sequestration ability of the system is inefficient.

CHAPTER FIVE:

CONCLUSIONS

Bomb-derived ^{14}C is distributed throughout the soil via root and microbial mixing. Using my model, it is possible to visualize how this younger carbon is transported to depth, resulting in $\Delta^{14}C$ concentrations earlier than that of true deposition. A decline in excess ^{210}Pb activity in the sediment indicates that ^{210}Pb did not migrate after being deposited, thus establishing an age-depth relationship that can be used to examine younger carbon movement to depth. In all systems of this study, I detected ^{14}C concentrations (Fm > 1) in sediments that were ^{210}Pb-dated to before the onset of bomb testing (1937-1892 CE). Given that the peak of thermonuclear weapons testing occurred in 1963, post-depositional movement of younger carbon must have occurred.

Inundation within the system allows the movement and export of carbon from the system, which could help explain why the salt marsh and mangrove systems had high export values. Increases in tidal activity or rainfall affect the amount of carbon exported from the system (Twilley, 1988; Twilley et al., 1992). Cores in this study were taken during a month that saw higher than average rainfall, which could explain why there was a high export value from the basin mangrove system. Assuming the cores taken are indicative of the system, riverine mangroves in the Ten Thousand Islands store more carbon in the soil, by an order of magnitude, than basin mangrove systems and salt marsh systems. Peat has been forming longer in the Ten Thousand Islands than Charlotte Harbor, so it makes sense that more carbon has been produced in that area. When comparing the amount of carbon produced to the amount of carbon stored, all systems stored less

than 1.05% of the carbon that was produced in the sediment. Given the definition of efficiency used in this study, the blue carbon ecosystems should be classified as inefficient.

Blue carbon ecosystems are regarded as efficient in carbon sequestration for several reasons, including particle trapping, sequestration of carbon into plant biomass, and the ability to store both allochthonous and autochthonous carbon. Despite this, blue carbon systems are generally net emitters of CO_2 and CH_4 to the atmosphere (Alongi, 2005), which may act as an offset to burial (Maher et al., 2018). Sedimentary CO_2 efflux and DIC export via tidal pumping are major sinks to the coastal ocean (Bouillon et al., 2008). In the model, I assumed all carbon loss from the system was in the form of DIC, but future use of this model should account for changes in carbon speciation to determine if the values align with literature values.

Blue carbon systems are home to huge systems of roots and burrow that assist in carbon movement throughout the system and are generally dominated by advective porewater flux. Based on the calculated Péclet number, I chose to use an advective model. The high Péclet number in the salt marsh system supports the use of an advective model, however, it's possible that the mangrove system could have benefitted from an advection-diffusion model. Given that the Péclet number in the mangrove systems was 1.26, which is just barely above the threshold of 1, it is possible that the inclusion of diffusion in the model could have resolved the ill fit of the model to study data.

Initial runs of the model demonstrated a completely efficient system, which is not realistic. Upon adding the reactive loss term, I still could not fit the model to the study data. The model also did not force a steady state and had no horizontal gradient built in. Though blue carbon systems exist in a non-steady state, perhaps the inclusion of a horizontal gradient could have helped to fit the model to the data. However, I believe that the inclusion of these changes would still not have made the model fit the data. I believe the ill fit of the model is more indicative of the inefficiencies

of the system, and not the inefficiencies of the model. As stated, carbon sequestration in blue carbon systems does not meet the definition of efficiency that was used in this study. All systems from this study have export values greater than 50%, meaning they cannot possibly be efficient because they cannot bury more carbon in the sediment than is being exported. When this is coupled with the fact that the systems in this study store less than 1.05% of the carbon produced, I believe blue carbon systems can be labeled effective in sequestering CO_2 from that atmosphere, but not efficient in burying it in long-term storage.

REFERENCES

Alongi, D.M. 2005. Mangrove-microbe-soil relations, *Interactions between macro-and microorganisms in marine sediments*: 85-103.

Alongi, D.M. 2009. *The energetics of mangrove forests* (Springer Science & Business Media).

Alongi, D.M. 2012. Carbon sequestration in mangrove forests, *Carbon management*, 3: 313-22.

Alongi, D.M. 2014. Carbon cycling and storage in mangrove forests, *Annual review of marine science*, 6: 195-219.

Alongi, D.M. 2020a. Carbon balance in salt marsh and mangrove ecosystems: A global synthesis, *Journal of Marine Science and Engineering*, 8: 767.

Alongi, D.M. 2020b. Carbon cycling in the world's mangrove ecosystems revisited: Significance of non-steady state diagenesis and subsurface linkages between the forest floor and the coastal ocean, *Forests*, 11: 977.

Alongi, D.M., Clough, B.F., Dixon, P., & Tirendi, F. 2003. Nutrient partitioning and storage in arid-zone forests of the mangroves Rhizophora stylosa and Avicenniamarina, *Trees*, 17: 51-60.

Alongi, D.M., Wattayakorn, G., Tirendi, F., & Dixon, P. 2004. Nutrient capital in different aged forests of the mangrove Rhizophora apiculata, *Botanica Marina*, 47: 116-24.

Appleby, P.G., & Oldfield, F. 1978. The calculation of lead-210 dates assuming a constant rate of supply of unsupported 210Pb to the sediment, *Catena*, 5: 1-8.

Bachand, P.A.M., Bachand, S., Fleck, J., Anderson, F., & Windham-Myers, L. 2014. Differentiating transpiration from evaporation in seasonal agricultural wetlands and the link to advective fluxes in the root zone, *Science of the Total Environment*, 484: 232-48.

Beaumont, N.J., Jones, L., Garbutt, A., Hansom, J.D., & Toberman, M. 2014. The value of carbon sequestration and storage in coastal habitats, *Estuarine, Coastal and Shelf Science*, 137: 32-40.

Beever III, J. , Gray, W. , Beever, L.B. , Cobb, D., & Walker, T. 2012. Climate change vulnerability assessment and adaptation opportunities for salt marsh types in Southwest Florida, *Southwest Florida Regional Planning Council. Fort Myers FL*.

Belokopytov, I.E., & Beresnevich, V.V. 1955. Giktorf's peat borers, *Torfyanaya Promyshlennost*, 8: 10.

Berner, R.A., & Raiswell, R. 1983. Burial of organic carbon and pyrite sulfur in sediments over Phanerozoic time: a new theory, *Geochimica et Cosmochimica Acta*, 47: 855-62.

Bianchi, T.S., Allison, M.A., Zhao, J., Li, X., Comeaux, R.S., Feagin, R.A., & Kulawardhana, R.W. 2013. Historical reconstruction of mangrove expansion in the Gulf of Mexico: linking climate change with carbon sequestration in coastal wetlands, *Estuarine, Coastal and Shelf Science*, 119: 7-16.

Bouillon, S., Borges, A.V., Castañeda-Moya, E., Diele, K., Dittmar, T., Duke, N.C., Kristensen, E., Lee, S.Y., Marchand, C., & Middelburg, J.J. 2008. Mangrove production and carbon sinks: a revision of global budget estimates, *Global biogeochemical cycles*, 22.

Bouillon, S., Middelburg, J.J., Dehairs, F., Borges, A.V., Abril, G., Flindt, M.R., Ulomi, S., & Kristensen, E. 2007. Importance of intertidal sediment processes and porewater exchange

on the water column biogeochemistry in a pristine mangrove creek (Ras Dege, Tanzania), *Biogeosciences*, 4: 311-22.

Breithaupt, J.L., Hurst, N., Steinmuller, H.E., Duga, E., Smoak, J.M., Kominoski, J.S., & Chambers, L.G. 2019. Comparing the biogeochemistry of storm surge sediments and pre-storm soils in coastal wetlands: Hurricane Irma and the Florida Everglades, *Estuaries and Coasts*, 43: 1090-103.

Breithaupt, J.L., Smoak, J.M., Bianchi, T.S., Vaughn, D., Sanders, C.J., Radabaugh, K.R., Osland, M.J., Feher, L.C., Lynch, J.C., & Cahoon, D.R. 2020. Increasing rates of carbon burial in southwest Florida coastal wetlands, *Journal of Geophysical Research: Biogeosciences*: e2019JG005349.

Breithaupt, J.L., Smoak, J.M., Rivera-Monroy, V.H., Castañeda-Moya, E., Moyer, R.P., Simard, M., & Sanders, C.J. 2017. Partitioning the relative contributions of organic matter and mineral sediment to accretion rates in carbonate platform mangrove soils, *Marine Geology*, 390: 170-80.

Breithaupt, J.L., Smoak, J.M., Smith III, T.J., & Sanders, C.J. 2014. Temporal variability of carbon and nutrient burial, sediment accretion, and mass accumulation over the past century in a carbonate platform mangrove forest of the Florida Everglades, *Journal of Geophysical Research: Biogeosciences*, 119: 2032-48.

Breithaupt, J.L., Smoak, J.M., Smith III, T.J., Sanders, C.J., & Hoare, A. 2012. Organic carbon burial rates in mangrove sediments: Strengthening the global budget, *Global biogeochemical cycles*, 26.

Cabral, A., Dittmar, T., Call, M., Scholten, J., de Rezende, C.E., Asp, N., Gledhill, M., Seidel, M., & Santos, I.R. 2021. Carbon and alkalinity outwelling across the groundwater-creek-shelf continuum off Amazonian mangroves, *Limnology and Oceanography Letters*.

Caçador, I., Costa, A.L., & Vale, C. 2004. Carbon storage in Tagus salt marsh sediments. in, *Biogeochemical Investigations of Terrestrial, Freshwater, and Wetland Ecosystems across the Globe* (Springer).

Castañeda-Moya, E., Twilley, R.R., & Rivera-Monroy, V.H. 2013. Allocation of biomass and net primary productivity of mangrove forests along environmental gradients in the Florida Coastal Everglades, USA, *Forest Ecology and Management*, 307: 226-41.

Chambers, L.G., Guevara, R., Boyer, J.N., Troxler, T.G., & Davis, S.E. 2016. Effects of salinity and inundation on microbial community structure and function in a mangrove peat soil, *Wetlands*, 36: 361-71.

Chambers, L.G., Osborne, T.Z., & Reddy, K.R. 2013. Effect of salinity-altering pulsing events on soil organic carbon loss along an intertidal wetland gradient: a laboratory experiment, *Biogeochemistry*, 115: 363-83.

Chatting, M., LeVay, L., Walton, M., Skov, M.W., Kennedy, H., Wilson, S., & Al-Maslamani, I. 2020. Mangrove carbon stocks and biomass partitioning in an extreme environment, *Estuarine, Coastal and Shelf Science*, 244: 106940.

Chen, G.C., Tam, N.F.Y., & Ye, Y. 2012. Spatial and seasonal variations of atmospheric N2O and CO2 fluxes from a subtropical mangrove swamp and their relationships with soil characteristics, *Soil Biology and Biochemistry*, 48: 175-81.

Chen, X., Santos, I.R., Call, M., Reithmaier, G.M.S., Maher, D.T., Holloway, C., Wadnerkar, P.D., Gómez-Álvarez, P., Sanders, C.J., & Li, L. 2021. The mangrove CO2 pump: Tidally driven pore-water exchange, *Limnology and Oceanography*, 66: 1563-77.

Chmura, G.L., Anisfeld, S.C, Cahoon, D.R., & Lynch, J.C. 2003. Global carbon sequestration in tidal, saline wetland soils, *Global biogeochemical cycles*, 17.

Chmura, G.L., & Hung, G.A. 2004. Controls on salt marsh accretion: A test in salt marshes of Eastern Canada, *Estuaries*, 27: 70-81.

Christian, R.R., Bryant Jr, W.L., & Brinson, M.M. 1990. Juncus roemerianus production and decomposition along gradients of salinity and hydroperiod, *Marine Ecology Progress Series*: 137-45.

Dittmar, T., Hertkorn, N., Kattner, G., & Lara, R.J. 2006. Mangroves, a major source of dissolved organic carbon to the oceans, *Global biogeochemical cycles*, 20.

Dodd, J.R., & Siemers, C.T. 1971. Effect of Late Pleistocene karst topography on Holocene sedimentation and biota, Lower Florida Keys, *Geological Society of America Bulletin*, 82: 211-18.

Donato, D.C., Kauffman, J.B., Murdiyarso, D., Kurnianto, S., Stidham, M., & Kanninen, M. 2011. Mangroves among the most carbon-rich forests in the tropics, *Nature Geoscience*, 4: 293-97.

Drake, K., Halifax, H., Adamowicz, S.C., & Craft, C. 2015. Carbon sequestration in tidal salt marshes of the Northeast United States, *Environmental management*, 56: 998-1008.

Duarte, C.M. 2017. Reviews and syntheses: Hidden forests, the role of vegetated coastal habitats in the ocean carbon budget, *Biogeosciences*, 14: 301-10.

Duarte, C.M., Marbà, N., Gacia, E., Fourqurean, J.W., Beggins, J., Barrón, C., & Apostolaki, E.T. 2010. Seagrass community metabolism: Assessing the carbon sink capacity of seagrass meadows, *Global biogeochemical cycles*, 24.

Duarte, C.M., Middelburg, J.J., & Caraco, N. 2005. Major role of marine vegetation on the oceanic carbon cycle, *Biogeosciences*, 2: 1-8.

Ewel, K., Twilley, R.R., & Ong, J.E. 1998. Different kinds of mangrove forests provide different goods and services, *Global Ecology & Biogeography Letters*, 7: 83-94.

Feagin, R.A., Mukherjee, N., Shanker, K., Baird, A.H., Cinner, J., Kerr, A.M., Koedam, N., Sridhar, A., Arthur, R., Jayatissa, L., Seen, D.L., Menon, M., Rodriguez, S., Shamsuddoha, M.D., & Dahdouh-Guebas, F. 2010. Shelter from the storm? Use and misuse of coastal vegetation bioshields for managing natural disasters, *Conservation Letters*, 3: 1-11.

Feller, I.C., Lovelock, C.E., Berger, U., McKee, K.L., Joye, S.B., & Ball, M.C. 2010. Biocomplexity in mangrove ecosystems, *Annual review of marine science*, 2: 395-417.

Flowers, T.J., & Colmer, T.D. 2008. Salinity tolerance in halophytes, *New phytologist*: 945-63.

Flowers, T.J., Hajibagheri, M.A., & Clipson, N.J.W. 1986. Halophytes, *The quarterly review of biology*, 61: 313-37.

Flowers, T.J., Troke, P.F., & Yeo, A.R. 1977. The mechanism of salt tolerance in halophytes, *Annual review of plant physiology*, 28: 89-121.

Friedrichs, C.T., & Perry, J.E. 2001. Tidal salt marsh morphodynamics: a synthesis, *Journal of Coastal Research*: 7-37.

Gacia, E., & Duarte, C.M. 2001. Sediment retention by a Mediterranean Posidonia oceanica meadow: the balance between deposition and resuspension, *Estuarine, Coastal and Shelf Science*, 52: 505-14.

Gerlach, M.J., Engelhart, S.E., Kemp, A.C., Moyer, R.P., Smoak, J.M., Bernhardt, C.E., & Cahill, N. 2017. Reconstructing Common Era relative sea-level change on the Gulf Coast of Florida, *Marine Geology*, 390: 254-69.

Hansen, J.C.R., & Reidenbach, M.A. 2012. Wave and tidally driven flows in eelgrass beds and their effect on sediment suspension, *Marine Ecology Progress Series*, 448: 271-87.
Hansen, V.D., & Nestlerode, J.A. 2014. Carbon sequestration in wetland soils of the northern Gulf of Mexico coastal region, *Wetlands Ecology and Management*, 22: 289-303.
Hemingway, J.D., Rothman, D.H., Grant, K.E., Rosengard, S.Z., Eglinton, T.I., Derry, L.A., & Galy, V.V. 2019. Mineral protection regulates long-term global preservation of natural organic carbon, *Nature*, 570: 228.
Himes-Cornell, A., Pendleton, L., & Atiyah, P. 2018. Valuing ecosystem services from blue forests: A systematic review of the valuation of salt marshes, sea grass beds and mangrove forests, *Ecosystem services*, 30: 36-48.
Ho, D.T., Ferrón, S., Engel, V.C., Anderson, W.T., Swart, P.K., Price, R.M., & Barbero, L. 2017. Dissolved carbon biogeochemistry and export in mangrove-dominated rivers of the Florida Everglades, *Biogeosciences*, 14: 2543-59.
Hollins, S.E., Ridd, P.V., & Read, W.W. 2000. Measurement of the diffusion coefficient for salt in salt flat and mangrove soils, *Wetlands Ecology and Management*, 8: 257-62.
Hua, Q., & Barbetti, M. 2004. Review of tropospheric bomb 14C data for carbon cycle modeling and age calibration purposes, *Radiocarbon*, 46: 1273-98.
Jenkins, W.J. 2003. Tracers of ocean mixing, *The Oceans and Marine Geochemistry*: 223-46.
Jennerjahn, T.C., & Ittekkot, V. 2002. Relevance of mangroves for the production and deposition of organic matter along tropical continental margins, *Naturwissenschaften*, 89: 23-30.
Jowsey, P.C. 1966. An improved peat sampler, *New phytologist*, 65: 245-48.
Kadlec, R.H. 2000. The inadequacy of first-order treatment wetland models, *Ecological Engineering*, 15: 105-19.
Kelleway, J.J., Saintilan, N., Macreadie, P.I., Skilbeck, C.G., Zawadzki, A., & Ralph, P.J. 2016. Seventy years of continuous encroachment substantially increases 'blue carbon'capacity as mangroves replace intertidal salt marshes, *Global change biology*, 22: 1097-109.
Komiyama, A., Ong, J.E., & Poungparn, S. 2008. Allometry, biomass, and productivity of mangrove forests: A review, *Aquatic botany*, 89: 128-37.
Koretsky, C.M., Meile, C., & Van Cappellen, P. 2002. Quantifying bioirrigation using ecological parameters: A stochastic approach, *Geochemical Transactions*, 3: 17-30.
Krauss, K.W., From, A.S., Doyle, T.W., Doyle, T.J., & Barry, M.J. 2011. Sea-level rise and landscape change influence mangrove encroachment onto marsh in the Ten Thousand Islands region of Florida, USA, *Journal of Coastal Conservation*, 15: 629-38.
Kristensen, E. 2008a. Mangrove crabs as ecosystem engineers; with emphasis on sediment processes, *Journal of sea Research*, 59: 30-43.
Kristensen, E., & Alongi, D.M. 2006. Control by fiddler crabs (Uca vocans) and plant roots (Avicennia marina) on carbon, iron, and sulfur biogeochemistry in mangrove sediment, *Limnology and Oceanography*, 51: 1557-71.
Kristensen, E., Bouillon, S., Dittmar, T., & Marchand, C. 2008b. Organic carbon dynamics in mangrove ecosystems: a review, *Aquatic botany*, 89: 201-19.
Kristensen, E., Mangion, P., Tang, M., Flindt, M.R., Holmer, M., & Ulomi, S. 2011. Microbial carbon oxidation rates and pathways in sediments of two Tanzanian mangrove forests, *Biogeochemistry*, 103: 143-58.
Krom, M.D., & Berner, R.A. 1980. Adsorption of phosphate in anoxic marine sediments 1, *Limnology and Oceanography*, 25: 797-806.

Kruczynski, W.L., Subrahmanyam, C.B., & Drake, S.H. 1978. Studies on the plant community of a North Florida salt marsh part I. primary production, *Bulletin of Marine Science*, 28: 316-34.

Kutschera, W. 2022. The versatile uses of the 14C bomb peak, *Radiocarbon*: 1-14.

Lee, J.S., & Kim, J.W. 2018. Dynamics of zonal halophyte communities in salt marshes in the world, *Journal of Marine and Island Cultures*, 7: 84-106.

Lee, S.Y., Primavera, J.H., Dahdouh-Guebas, F., McKee, K.L., Bosire, Jared O., Cannicci, S., Diele, K., Fromard, F., Koedam, N., & Marchand, C. 2014. Ecological role and services of tropical mangrove ecosystems: a reassessment, *Global Ecology and Biogeography*, 23: 726-43.

Leopold, A., Marchand, C., Deborde, J., & Allenbach, M. 2015. Temporal variability of CO2 fluxes at the sediment-air interface in mangroves (New Caledonia), *Science of the Total Environment*, 502: 617-26.

Lo Iacono, C., Mateo, M.A., Gracia, E., Guasch, L., Carbonell, R., Serrano, L., Serrano, O., & Danobeitia, J. 2008. Very high-resolution seismo-acoustic imaging of seagrass meadows (Mediterranean Sea): Implications for carbon sink estimates, *Geophysical Research Letters*, 35.

Lovelock, C.E., Simpson, L.T., Duckett, L.J., & Feller, I.C. 2015. Carbon budgets for Caribbean mangrove forests of varying structure and with phosphorus enrichment, *Forests*, 6: 3528-46.

Macreadie, P. I., Anton, A., Raven, J. A., Beaumont, N., Connolly, R. M., Friess, D. A., Kelleway, J. J., Kennedy, H., Kuwae, T., Lavery, P. S., Lovelock, C. E., Smale, D. A., Apostolaki, E. T., Atwood, T. B., Baldock, J., Bianchi, T. S., Chmura, G. L., Eyre, B. D., Fourqurean, J. W., Hall-Spencer, J. M., Huxham, M., Hendriks, I. E., Krause-Jensen, D., Laffoley, D., Luisetti, T., Marba, N., Masque, P., McGlathery, K. J., Megonigal, J. P., Murdiyarso, D., Russell, B. D., Santos, R., Serrano, O., Silliman, B. R., Watanabe, K., & Duarte, C. M. 2019. The future of blue carbon science, *Nature Communications*, 10: 1-16.

Maher, D.T., Call, M., Santos, I.R., & Sanders, C.J. 2018. Beyond burial: lateral exchange is a significant atmospheric carbon sink in mangrove forests, *Biology letters*, 14: 20180200.

Maher, D.T., Santos, I.R., Golsby-Smith, L., Gleeson, J., & Eyre, B.D. 2013. Groundwater-derived dissolved inorganic and organic carbon exports from a mangrove tidal creek: The missing mangrove carbon sink?, *Limnology and Oceanography*, 58: 475-88.

Maher, D.T., Santos, I.R., Schulz, K.G., Call, M., Jacobsen, G.E., & Sanders, C.J. 2017. Blue carbon oxidation revealed by radiogenic and stable isotopes in a mangrove system, *Geophysical Research Letters*, 44: 4889-96.

Maher, D.T., Sippo, J.Z., Tait, D.R., Holloway, C., & Santos, I.R. 2016. Pristine mangrove creek waters are a sink of nitrous oxide, *Scientific reports*, 6: 1-8.

Martinetto, P., Montemayor, D.I., Alberti, J., Costa, C.S.B., & Iribarne, O. 2016. Crab bioturbation and herbivory may account for variability in carbon sequestration and stocks in south west atlantic salt marshes, *Frontiers in Marine Science*, 3: 122.

Mazda, Y., Kobashi, D., & Okada, S. 2005. Tidal-scale hydrodynamics within mangrove swamps, *Wetlands Ecology and Management*, 13: 647-55.

McKee, K.L., Cahoon, D.R., & Feller, I.C. 2007. Caribbean mangroves adjust to rising sea level through biotic controls on change in soil elevation, *Global Ecology and Biogeography*, 16: 545-56.

McKenzie, L.J., Nordlund, L.M., Jones, B.L., Cullen-Unsworth, L.C., Roelfsema, C., & Unsworth, Richard K.F. 2020. The global distribution of seagrass meadows, *Environmental Research Letters*, 15: 074041.

Mcleod, E., Chmura, G.L., Bouillon, S., Salm, R., Björk, M., Duarte, C.M., Lovelock, C.E., Schlesinger, W.H., & Silliman, B.R. 2011. A blueprint for blue carbon: toward an improved understanding of the role of vegetated coastal habitats in sequestering CO2, *Frontiers in Ecology and the Environment*, 9: 552-60.

Mitra, S., Wassmann, R., & Vlek, P.L.G. 2005. An appraisal of global wetland area and its organic carbon stock, *Current Science*, 88: 25-35.

Murray, R.H., Erler, D.V., & Eyre, B.D. 2015. Nitrous oxide fluxes in estuarine environments: response to global change, *Global change biology*, 21: 3219-45.

Najjar, R.G., Herrmann, M., Alexander, R., Boyer, E.W., Burdige, D.J., Butman, D., Cai, W.J., Canuel, E.A., Chen, R.F., & Friedrichs, M.A.M. 2018. Carbon budget of tidal wetlands, estuaries, and shelf waters of Eastern North America, *Global biogeochemical cycles*, 32: 389-416.

Nellemann, C., Corcoran, E., Duarte, C.M., Valdes, L., De Young, C., Fonseca, L., & Grimsditch, G. 2009. *Blue carbon: the role of healthy oceans in binding carbon: a rapid response assessment* (UNEP/Earthprint).

Nydal, R., & Lövseth, K. 1965. Distribution of radiocarbon from nuclear tests, *Nature*, 206: 1029-31.

Ouyang, X., & Lee, S.Y. 2013. Carbon accumulation rates in salt marsh sediments suggest high carbon storage capacity, *Biogeosciences Discussions*, 10: 19,155-88.

Ouyang, X., & Lee, S.Y. 2014. Updated estimates of carbon accumulation rates in coastal marsh sediments, *Biogeosciences*, 11: 5057-71.

Ouyang, X., Lee, S.Y., & Connolly, R.M. 2017. The role of root decomposition in global mangrove and saltmarsh carbon budgets, *Earth-Science Reviews*, 166: 53-63.

Parkinson, R.W. 1989. Decelerating Holocene sea-level rise and its influence on Southwest Florida coastal evolution; a transgressive/regressive stratigraphy, *Journal of Sedimentary Research*, 59: 960-72.

Pendleton, L., Donato, D.C., Murray, B.C., Crooks, S., Jenkins, W.A., Sifleet, S., Craft, C., Fourqurean, J.W., Kauffman, J.B., & Marbà, N. 2012. Estimating global "blue carbon" emissions from conversion and degradation of vegetated coastal ecosystems, *PloS one*, 7: e43542.

Persico, E.P., Sharp, S.J., & Angelini, C. 2017. Feral hog disturbance alters carbon dynamics in southeastern US salt marshes, *Marine Ecology Progress Series*, 580: 57-68.

Poffenbarger, H.J., Needelman, B.A., & Megonigal, J.P. 2011. Salinity influence on methane emissions from tidal marshes, *Wetlands*, 31: 831-42.

Radabaugh, K.R., Moyer, R.P., Chappel, A.R., Dontis, E.E., Russo, C.E., Joyse, K.M., Bownik, M.W., Goeckner, A.H., & Khan, N.S. 2019. Mangrove damage, delayed mortality, and early recovery following Hurricane Irma at two landfall sites in Southwest Florida, USA, *Estuaries and Coasts*, 43: 1104-18.

Radabaugh, K.R., Powell, C.E., & Moyer, R.P. 2017. Coastal Habitat Integrated Mapping and Monitoring Program Report for the State of Florida.

Ray, R., Baum, A., Rixen, T., Gleixner, G., & Jana, T.K. 2018. Exportation of dissolved (inorganic and organic) and particulate carbon from mangroves and its implication to the carbon budget in the Indian Sundarbans, *Science of the Total Environment*, 621: 535-47.

Redelstein, R., Dinter, T., Hertel, D., & Leuschner, C. 2018. Effects of inundation, nutrient availability and plant species diversity on fine root mass and morphology across a saltmarsh flooding gradient, *Frontiers in plant science*, 9: 98.

Reithmaier, G.M.S., Ho, D.T., Johnston, S.G., & Maher, D.T. 2020. Mangroves as a Source of Greenhouse Gases to the Atmosphere and Alkalinity and Dissolved Carbon to the Coastal Ocean: A Case Study from the Everglades National Park, Florida, *Journal of Geophysical Research: Biogeosciences*, 125: e2020JG005812.

Reithmaier, G.M.S., Johnston, S.G., Junginger, T., Goddard, M.M., Sanders, C.J., Hutley, L.B., Ho, D.T., & Maher, D.T. 2021. Alkalinity production coupled to pyrite formation represents an unaccounted blue carbon sink, *Global biogeochemical cycles*, 35: e2020GB006785.

Rosenheim, B.E., Day, M.B., Domack, E., Schrum, H., Benthien, A., & Hayes, J.M. 2008. Antarctic sediment chronology by programmed-temperature pyrolysis: Methodology and data treatment, *Geochemistry, Geophysics, Geosystems*, 9: 1-16.

Rosentreter, J.A., Al-Haj, A.N., Fulweiler, R.n W., & Williamson, P. 2021. Methane and nitrous oxide emissions complicate coastal blue carbon assessments, *Global biogeochemical cycles*, 35: e2020GB006858.

Rosentreter, J.A., Maher, D.T., Erler, D.V., Murray, R.H., & Eyre, B.D. 2018a. Seasonal and temporal CO2 dynamics in three tropical mangrove creeks–A revision of global mangrove CO2 emissions, *Geochimica et Cosmochimica Acta*, 222: 729-45.

Rosentreter, J.A., Maher, D.T., Erler, D.V., Murray, R.H., & Eyre, B.D. 2018b. Methane emissions partially offset “blue carbon” burial in mangroves, *Science advances*, 4: eaao4985.

Saintilan, N., Rogers, K., Mazumder, D., & Woodroffe, C. 2013. Allochthonous and autochthonous contributions to carbon accumulation and carbon store in southeastern Australian coastal wetlands, *Estuarine, Coastal and Shelf Science*, 128: 84-92.

Santos, I.R., Burdige, D.J., Jennerjahn, T.C., Bouillon, S., Cabral, A., Serrano, O., Wernberg, T., Filbee-Dexter, K., Guimond, J., & Tamborski, J.J. 2021. The renaissance of Odum's outwelling hypothesis in 'Blue Carbon' science, *Estuarine, Coastal and Shelf Science*: 107361.

Santos, I.R., Eyre, B.D., & Huettel, M. 2012. The driving forces of porewater and groundwater flow in permeable coastal sediments: A review, *Estuarine, Coastal and Shelf Science*, 98: 1-15.

Santos, I.R., Maher, D.T., Larkin, R., Webb, J.R., & Sanders, C.J. 2019. Carbon outwelling and outgassing vs. burial in an estuarine tidal creek surrounded by mangrove and saltmarsh wetlands, *Limnology and Oceanography*, 64: 996-1013.

Schafer, C. 2020. Mechanisms of carbon movement and stabilization in mangrove wetlands, University of South Florida.

Scudlark, J.R., & Church, T.M. 1989. The sedimentary flux of nutrients at a Delaware salt marsh site: A geochemical perspective, *Biogeochemistry*, 7: 55-75.

Shier, D.E. 1969. Vermetid reefs and coastal development in the Ten Thousand Islands, southwest Florida, *Geological Society of America Bulletin*, 80: 485-508.

Sippo, J.Z., Maher, D.T., Tait, D.R., Ruiz-Halpern, S., Sanders, C.J., & Santos, I.R. 2017. Mangrove outwelling is a significant source of oceanic exchangeable organic carbon, *Limnology and Oceanography Letters*, 2: 1-8.

Smoak, J.M., Breithaupt, J.L., Smith III, T.J., & Sanders, C.J. 2013. Sediment accretion and organic carbon burial relative to sea-level rise and storm events in two mangrove forests in Everglades National Park, *Catena*, 104: 58-66.

Spivak, A.C., Sanderman, J., Bowen, J.L., Canuel, E.A., & Hopkinson, C.S. 2019. Global-change controls on soil-carbon accumulation and loss in coastal vegetated ecosystems, *Nature Geoscience*, 12: 685-92.

Steinmuller, H.E., Foster, T.E., Boudreau, P., Hinkle, C.R., & Chambers, L.G. 2020. Tipping points in the mangrove march: characterization of biogeochemical cycling along the mangrove-salt marsh ecotone, *Ecosystems*: 1-18.

Stout, J.P. 1978. *An analysis of annual growth and productivity of Juncus roemerianus scheele and Spartina alterniflora loisel in coastal Alabama* (The University of Alabama).

Subt, C., Yoon, H. I., Yoo, K. C., Lee, J. I., Leventer, A., Domack, E. W., & Rosenheim, B. E. 2017. Sub-ice shelf sediment geochronology utilizing novel radiocarbon methodology for highly detrital sediments, *Geochemistry, Geophysics, Geosystems*, 18: 1404-18.

Taylor, J.L. 1974. The Charlotte Harbor estuarine system, *Florida Scientist*: 205-16.

Trumbore, S. 2009. Radiocarbon and soil carbon dynamics, *Annual Review of Earth and Planetary Sciences*, 37: 47-66.

Turner, R.E., Howes, B.L., Teal, J.M., Milan, C.S., Swenson, E.M., & Goehringer-Toner, D.D. 2009. Salt marshes and eutrophication: An unsustainable outcome, *Limnology and Oceanography*, 54: 1634-42.

Twilley, R.R. 1985. The exchange of organic carbon in basin mangrove forests in a southwest Florida estuary, *Estuarine, Coastal and Shelf Science*, 20: 543-57.

Twilley, R.R. 1988. Coupling of mangroves to the productivity of estuarine and coastal waters. in, *Coastal-offshore ecosystem interactions* (Springer).

Twilley, R.R., Castañeda-Moya, E., Rivera-Monroy, V.H., & Rovai, A. 2017. Productivity and carbon dynamics in mangrove wetlands. in, *Mangrove ecosystems: A global biogeographic perspective* (Springer).

Twilley, R.R., Chen, R.H., & Hargis, T. 1992. Carbon sinks in mangroves and their implications to carbon budget of tropical coastal ecosystems, *Water, Air, and Soil Pollution*, 64: 265-88.

Twilley, R.W., Lugo, A.E., & Patterson-Zucca, C. 1986. Litter production and turnover in basin mangrove forests in southwest Florida, *Ecology*, 67: 670-83.

Ungar, I.A. 1998. Are biotic factors significant in influencing the distribution of halophytes in saline habitats?, *The botanical review*, 64: 176-99.

Wang, F., Sanders, C.J., Santos, I.R., Tang, J., Schuerch, M., Kirwan, M.L., Kopp, R.E., Zhu, K., Li, X., & Yuan, J. 2021. Global blue carbon accumulation in tidal wetlands increases with climate change, *National Science Review*.

Wang, Y., Amundson, R., & Trumbore, S.E. 1996. Radiocarbon dating of soil organic matter, *Quaternary Research*, 45: 282-88.

Wilkie, L., O'Hare, M.T., Davidson, I., Dudley, B., & Paterson, D.M. 2012. Particle trapping and retention by Zostera noltii: A flume and field study, *Aquatic botany*, 102: 15-22.

Wolanski, E. 1995. Transport of sediment in mangrove swamps. In *Asia-Pacific Symposium on Mangrove Ecosystems*, 31-42. Springer.

Xiao, K., Wilson, A.M., Li, H., & Ryan, C. 2019. Crab burrows as preferential flow conduits for groundwater flow and transport in salt marshes: A modeling study, *Advances in Water Resources*, 132: 103408.

Xiao, K., Wilson, A.M., Li, H., Santos, I.R., Tamborski, J.J., Smith, E., Lang, S.Q., Zheng, C., Luo, X., & Lu, M. 2021. Large CO2 release and tidal flushing in salt marsh crab burrows reduce the potential for blue carbon sequestration, *Limnology and Oceanography*, 66: 14-29.

Zedler, J.B., & Kercher, S. 2005. Wetland resources: status, trends, ecosystem services, and restorability, *Annu. Rev. Environ. Resour.*, 30: 39-74.

APPENDIX A:

LEAD-210, RADIOCARBON, AND STABLE CARBON ISOTOPIC DATA

Table 4. *Sedimentary analysis for Excess ^{210}Pb (dpm/g) of the salt marsh site.*

Depth (cm)	Excess Pb-210 Activity (dpm/g)	Excess Pb-210 Activity Error	Age at given depth (yr)	Age Error (yr)	Sedimentation Rate (mg cm^{-2} yr-1)	Carbon density (g cm^{-3})	OC (%)
0-1	24.93	0.69	7.82	0.51	14.81	0.031	33.37
1-2	20.24	0.61	14.64	0.57	14.52	0.045	38.48
2-3	21.85	0.74	23.33	0.67	10.58	0.043	41.13
3-4	12.80	0.52	29.52	0.77	14.29	0.041	39.09
4-5	8.04	0.32	33.39	0.84	19.44	0.048	41.14
5-6	7.88	0.42	41.66	0.99	16.45	0.043	43.04
6-7	7.06	0.46	47.89	1.13	14.64	0.048	40.26
7-8	6.24	0.36	57.19	1.39	13.02	0.029	40.29
8-9	5.35	0.47	63.92	1.60	11.83	0.036	41.77
9-10	3.89	0.23	70.56	1.92	13.18	0.036	43.30
10-11	3.32	0.25	78.02	2.35	12.44	0.042	41.47
11-12	3.59	0.34	88.58	3.07	8.71	0.049	42.41
12-13	3.45	0.37	107.01	4.81	5.81	0.042	38.99
13-14	1.74	0.29	128.91	8.02	6.18	0.057	42.17

Table 5. *Lead-210, radiocarbon (^{14}C) and stable carbon isotopic ($\delta^{13}C$) data for the salt marsh site. Fm denotes fraction modern.*

Interval (cm)	^{210}Pb Date Interval	OC (%)	OC Burial (g m^{-2} y^{-1})	Mass Sed Rate (mg cm^{-2} y^{-1})	Accretion (mm y^{-1})	DBD	Carbon density (g cm^{-3})	Fm	Fm error	Δ14C	Δ14C error	δ13C (‰)
0-1	2007-2015	33.37	49.44	14.81	1.28	0.09	0.03					
1-2	2001-2007	38.48	55.86	14.52	1.47	0.12	0.04					
2-3	1992-2001	41.13	43.5	10.58	1.15	0.1	0.04					
3-4	1986-1992	39.09	55.86	14.29	1.62	0.11	0.04	1.22	0.0024	219.5	217.1	-27.27
4-5	1982-1986	41.14	79.99	19.44	2.59	0.12	0.05	1.25	0.0025	251.5	249.0	-27.22
5-6	1974-1982	43.04	70.8	16.45	1.21	0.1	0.04	1.25	0.0025	250.9	248.4	-27.14
6-7	1967-1974	40.26	58.94	14.64	1.61	0.12	0.05					
7-8	1958-1967	40.29	52.46	13.02	1.07	0.07	0.03					
8-9	1951-1958	41.77	49.4	11.83	1.49	0.09	0.04					
9-10	1945-1951	43.3	57.1	13.18	1.51	0.08	0.04	1.12	0.0021	115.2	113.1	-26.7
10-11	1937-1945	41.47	51.58	12.44	1.34	0.1	0.04					
11-12	1927-1937	42.41	36.92	8.71	0.95	0.11	0.05					
12-13	1908-1927	38.99	22.64	5.81	0.54	0.11	0.04					
13-14	1886-1908	42.17	26.05	6.18	0.46	0.13	0.06					
14-15		37.5				0.14	0.05	1.01	0.0025	5.7	3.2	-25.06
20-21		37.6				0.12	0.05	1.00	0.0019	-4.9	-6.8	-27.07

Table 6. *Lead-210, radiocarbon (^{14}C) and stable carbon isotopic ($\delta^{13}C$) data for the riverine mangrove site. Fm denotes fraction modern.*

Interval (cm)	^{210}Pb Date Interval	OC (%)	OC Burial (g m^{-2} y^{-1})	Mass Sed Rate (mg cm^{-2} y^{-1})	Accretion (mm y^{-1})	DBD	Carbon density (g cm^{-3})	Fm	Fm Blank Corrected	Δ14C	$\delta^{13}C$ (‰)
0-2	2012-2017	21.92	145.89	66.56	3.60	1.92	0.42				
2-4	2008-2012	20.70	143.64	69.39	4.62	1.98	0.41				
4-6	2003-2008	19.95	125.15	62.74	4.81	1.99	0.40				
6-8	1999-2003	19.21	133.15	69.32	4.28	1.98	0.38	1.11	1.12	110.06	-29.01
8-10	1993-1999	17.67	116.93	66.19	3.50	1.76	0.31				
10-11	1990-1993	17.04	104.49	61.34	2.96	1.83	0.31	1.12	1.13	121.77	-29.97
11-12	1986-1990	18.26	97.08	53.17	2.83	1.74	0.32				
12-13	1982-1986	16.30	87.12	53.43	2.34	2.18	0.36				
13-14	1978-1982	20.02	100.29	50.10	2.83	1.82	0.36	1.14	1.15	135.45	-28.77
14-15	1974-1978	13.83	68.22	49.32	2.42	1.97	0.27				
15-16	1970-1974	18.54	91.43	49.32	2.30	2.01	0.37				
16-17	1966-1970	16.26	77.33	47.56	2.33	1.97	0.32	1.13	1.14	129.17	-28.79
17-18	1962-1966	15.67	75.37	48.10	2.80	1.83	0.29				
18-19	1956-1962	16.63	62.60	37.65	1.81	1.73	0.29				
19-20	1951-1956	19.33	68.13	35.24	1.79	1.91	0.37				
20-21	1943-1951	15.31	45.18	29.51	1.30	1.70	0.26				
21-22	1935-1943	19.06	52.80	27.70	1.23	1.84	0.35				
22-23	1925-1935	14.28	32.69	22.90	1.01	1.97	0.28				
23-24	1912-1925	14.56	25.14	17.26	0.77	1.65	0.24				
24-25	1892-1912	13.91	19.54	14.05	0.48	1.76	0.25	1.07	1.08	74.35	-28.86
25-26	1861-1892	16.72	11.85	7.09	0.33	2.16	0.36				

Table 7. *Lead-210, radiocarbon (^{14}C) and stable carbon isotopic ($\delta^{13}C$) data for the basin mangrove site. Fm denotes fraction modern.*

Interval (cm)	^{210}Pb Date Interval	OC (%)	OC Burial (g m^{-2} y^{-1})	Mass Sed Rate (mg cm^{-2} y^{-1})	Accretion (mm y^{-1})	DBD	Carbon density (g cm^{-3})	Fm	Fm Blank Corrected	Δ14C	$\delta^{13}C$ (‰)
0-2	2013-2017	28.96	97.34	33.61	4.21	0.16	0.05				
2-4	2009-2013	28.01	112.45	40.15	4.94	0.16	0.05				
4-6	2004-2009	25.95	96.21	37.08	4.40	0.17	0.04	1.09	1.09	88.70	-27.39
6-8	2001-2004	26.22	135.86	51.82	5.87	0.18	0.05				
8-10	1997-2001	25.03	125.51	50.14	4.87	0.21	0.05				
10-11	1993-1997	22.83	126.73	55.51	2.46	0.23	0.05				
11-12	1989-1993	20.99	138.78	66.12	3.19	0.21	0.04				
12-13	1986-1989	19.78	112.56	56.91	3.15	0.18	0.04	1.17	1.15	165.33	-28.56
13-14	1980-1986	22.06	86.56	39.24	1.57	0.25	0.06				
14-15	1975-1980	11.82	58.38	49.39	1.88	0.26	0.03				
15-16	1971-1980	4.89	31.40	64.16	2.51	0.26	0.01	1.14	1.15	136.18	-28.56
16-17	1964-1971	25.97	106.83	41.14	1.60	0.26	0.07				
17-18	1957-1964	5.06	21.32	42.11	1.33	0.32	0.02	1.08	1.08	78.28	-28.72
18-19	1952-1957	13.77	73.41	53.31	2.13	0.25	0.03				
19-20	1946-1952	7.29	34.19	46.93	1.60	0.29	0.02				
20-21	1930-1946	21.88	69.22	31.64	0.62	0.51	0.11	1.04	1.05	38.70	-29.49
21-22	1916-1930	6.49	27.18	41.90	0.75	0.56	0.04				
22-23	1911-1916	4.90	31.81	64.92	1.72	0.38	0.02	1.01	1.01	6.12	-28.80
23-24	1888-1911	2.02	5.13	25.36	0.45	0.57	0.01				
24-25	1878-1888	4.99	20.81	41.69	0.95	0.44	0.02				

Table 8. *Calculation of carbon produced and stored in the salt marsh, riverine mangrove, and basin mangrove sites. The amount of carbon produced was calculated by multiplying peat age, area, and net primary production (NPP). The amount of carbon stored was calculated by multiplying area by the amount of carbon stored in the core.*

	Peat age (yrs)	Area (ha)	NPP (Mg ha^{-1} y^{-1})	Mg C produced	Total C in core section (Mg ha^{-1})	Mg C stored	C stored/C produced	% C stored
Salt Marsh	2180 §	6011 ¤	17.6 ‡	2.31E+08	59.03	3.55E+05	0.002	0.15
Riverine Mangrove	3500 *	7281 †	19.20 ∴	4.89E+08	691.75	5.04E+06	0.010	1.03
Basin Mangrove	3500 *	7281 †	19.20 ∴	4.89E+08	80.11	5.83E+05	0.001	0.12

* Parkinson, 1989
† Krauss et al., 2011
§ Gerlach et al., 2017
¤ Beever et al., 2012
‡ Alongi 2020a
∴ Castañeda-Moya et al., 2013

APPENDIX B:

SENSITIVITY TESTS USING THE SWAMPY PACKAGE

The SwamPy (.py file) package was developed by my advisor, Brad Rosenheim, and is designed to do simple iterative calculations of advection based on the ^{210}Pb years obtained from the data sets for each system. My role was to develop sensitivity tests for the SwamPy package using Jupyter Notebook (.ipynb file) that would test the method of mixdown and how that affects the amount of carbon that is mixed to depth.

SWAMPY PACKAGE

```
#Module for advection model of mangrove and marsh below-ground carbon flux
from logging import root
import math
from turtle import down
from numpy.lib.arraypad import pad
import pandas as pd
import numpy as np
import matplotlib.pyplot as plt

print('********** swamPy Advective Model Functions **********')

DEBUG = False

def debug(*args):
    '''
    Print argument if DEBUG is set to True
    '''
    if DEBUG == True:
        print(*args)

def square_wave(attenuation_length, max_proportion):
    '''
```

```
    Returns list of equal proportions of mixing (from the increment above), length equal to the
    attenuation length, or the depth to which analytes can be transported in the core.

      Inputs:
          attenuation_length - The number of increments over which the square wave propagates.
          Function does not determine if the increments are in time or length units.
          max_proportion - The amount of material from above that can mix down into the
          increment below. Scalar between 0 and 1.
      Outputs:
         square_out - floats equal to the max_proportion in a list of length of attenuation length

  '''
  #Check that inputs are within limits, correct if not
  if max_proportion > 1:
     max_proportion = 0.9
     print(
        'Maximum proportion cannot be greater than 1! Changed to\n',
        'max_proportion = 0.9.'
     )
  elif max_proportion < 0:
     max_proportion = 0.1
     print(
       'Maximum proportion cannot be less than 0! Changed to\n',
        'max_proportion = 0.1.'
     )
  square_out =  [max_proportion]*attenuation_length

  return square_out

def Gauss_mix_down(attenuation_length, max_proportion):
  '''
  Returns list of of mixing proportions reflective of a half-Gaussian distribution.
  Function calculates the Gaussian starting at the center (maximum) and then falls down the falling
  limb of the Gaussian curve.

      Inputs:
          attenuation_length - The number of increments over which the square wave propagates.
          Function does not determine if the increments are in time or length units.
          max_proportion - scalar defining the maximum of the Gaussian distribution; mixing
          proportions will decrease from this number. Number should be between 0 and 1.
      Outputs:
         square_out - floats equal to the max_proportion in a list of length of attenuation length

  '''
```

```
    #Check that inputs are within limits, correct if not
    if max_proportion > 1:
        max_proportion = 0.6
        print(
            'You entered a maximum mix-down proportion greater than 1!\n',
            'Value was changed to max_proportion = 0.6, and Gaussian calculated\n',
            'for output values'
        )
    elif max_proportion < 0:
        max_proportion = 0.1
        print(
            'You entered a maximum mix-down proportion less than 0!\n',
            'Value was changed to max_proportion = 0.1, and Gaussian calculated\n',
            'for output values'
        )

    c = 20*attenuation_length
    Gauss_out = [max_proportion*math.exp(-((n-0)**2)/(2*((attenuation_length/3)**2))) for n in
range(0, attenuation_length)]

    return Gauss_out

def annual_avg_bomb_curve(bombcurve_df):
    '''
      This function take the bomb curve data and interpolates it to yearly data averaging all data
      within a single calendar year.

        Inputs:
            bombcurve_df (DataFrame) - the loaded .csv with atmospheric bomb curve data. The
            columns accessed are 'Year_AD', 'Fm_mean', and 'D14C_mean'
        Outputs:
            averaged_df (DataFrame) - output DataFrame with indices of years and columns of D14C
            and Fm. The columns are yearly averages.
    '''
    #Set bounds of individual years.
    bgn=math.floor(min(bombcurve_df['Year_AD']))
    end=math.floor(max(bombcurve_df['Year_AD']))
    rng=round(end-bgn,0)
    debug('Range in years is ', rng, ' from ', bgn, ' to ', end)
    #Create empty container dataframe for yearly averaged data:
    averaged_df=pd.DataFrame(
        [],
        index=np.linspace(bgn, end, rng+1),
        columns=['D14C','Fm']
```

```
    )
    #For loop to fill the DataFrame container:
    for Y in averaged_df.index:
        debug('Working on year ', Y)
        Y1=math.floor(Y)
        Y2=math.floor(Y+1)
        bool_mask=(bombcurve_df['Year_AD']>=Y1) & (bombcurve_df['Year_AD']<=Y2)
        average_of_each_column_in_slice = bombcurve_df.loc[bool_mask].mean(axis=0)
        averaged_df.loc[Y].D14C=average_of_each_column_in_slice['D14C_mean']
        averaged_df.loc[Y].Fm=average_of_each_column_in_slice['Fm_mean']

    return averaged_df

def pad_timeseries(sedD14C_df, begin_year):
    '''
    This function pads the timeseries of D14C data. It is designed to work expressly with the output
    of the annual_avg_bomb_curve function, a DataFrame with index = Year_AD. This function
    could be modified to accept more diverse inputs with different types of time series.

        Inputs:
            sedD14C_df - DataFrame: This is the output of the annual_avg_bomb_curve function. The
            index of this DataFrame is year, so this function works expressly with that by making a
            new dataframe with the same type of index and concatenating them together.
            begin_year - Scalar: this is the year you wish to begin your dataset. The begin_year cannot
            be greater than the minimum year in the input DataFrame. If it is, the function returns a
            new DataFrame that is identical to the input dataframe.
    '''

    #Check to make sure the beginning year is before the earliest year in the dataset:
    if begin_year < min(sedD14C_df.index):
        debug('Padding data from ' + str(begin_year) + ' to ' + str(min(sedD14C_df.index)-1) + '.\n')
        diff = min(sedD14C_df.index) - begin_year - 1 #Minus one ensures no repeated index at the
minimum of the existing index
        debug('Creating linear interpolation between ' + str(begin_year) + ' and ' +
str(min(sedD14C_df.index)-1) + ' with ' + str(diff) + ' steps.')
        pad_ind = np.linspace(begin_year, min(sedD14C_df.index)-1, int(diff+1))
        #Add some randomness to the data for natural, unknown variability.
        pad_df=pd.DataFrame(np.full(len(pad_ind), np.random.randint(-260, -250,
len(pad_ind)))/10, index=pad_ind, columns=['D14C'])
       #UNDER CONSTRUCTION - Add decay function in case someone chooses to pad really far
back in time.
        pad_df['Fm'] = pad_df['D14C']/1000+1
        padded_df = pd.concat([sedD14C_df, pad_df]).sort_index()
    else:
```

```
        print('Variable begin_year is after the minimum year of the DataFrame.\n',
              'Not padding dataset.\n'
        )
        padded_df = sedD14C_df

    return padded_df

def viz_mixdown(increments, att_prop):
    '''
    This function plots the mixdown model and allows visualization.
        Inputs:
            Increments: (int) How many increments (time or distance) does carbon get mixed down?
           att_prop: (list of floats) output of either Gauss mixdown or square wave. List of proportions
            of material being mixed downward.
    '''
    _, ax=plt.subplots(nrows=1, ncols=1)
    xes=list(range(0, increments))
    xes_neg=list(range(-increments, 0))

    ax.plot(xes, att_prop, marker = '^', markersize = 10, mfc = 'yellow', mec = 'darkred', linestyle =
" )
    rev_output=reversed(att_prop)
    ax.plot(xes_neg, att_prop[::-1], color = 'lightblue')
    ax.plot(xes, att_prop, color = 'lightblue')
    ax.set_xlabel('Increment (time or length)')
    ax.set_ylabel('proportion mixed downward to next increment')

    return ax

def create_input_df(pad_to_year, input_14C_df, acc_rate, POC_productivity):
    '''
    Use the atmospheric bomb curve data to generate an input dataframe, then use the input
    dataframe to create an output dataframe. This function pads the atmospheric data and

    '''
    #Pad dataframe back to enough years to handle the downward mixing depth
    input_14C_df = pad_timeseries(input_14C_df, pad_to_year)
    debug('Padded time series back to ' + str(pad_to_year))

    #Calculate the depth of the core at given years using the sedimentation rate above.
    debug('Calculating depth and mass of organic carbon produced yearly...')
    depth = pd.DataFrame(np.multiply((input_14C_df.index-max(input_14C_df.index)),acc_rate),
index=input_14C_df.index, columns=['depth'])
```

```
    mOC_per_year = pd.DataFrame(np.full(len(depth), POC_productivity),
index=input_14C_df.index, columns=['mOC'])

    #Join dataframes and add columns to receive the output values in a new dataframe
    output_14C_df = input_14C_df.join([depth['depth'], mOC_per_year['mOC']], how='outer')
    new_cols = float('NaN') * output_14C_df['depth']
    new_col_names = ['mOC_out', 'D14C_out', 'OC_export_mass', 'OC_export_D14C']
    for name in new_col_names:
        output_14C_df[name] = new_cols

    debug(output_14C_df.head())

    return output_14C_df

def model_interator_time(
    sedD14C_df,
    mix_time,
    pad_to_year,
    acc_rate,
    POC_productivity,
    alpha=1,
    epsilon=0,
    root_shunt=0
):
    '''
    This function iterates the model. Functionalizing allows one line modeling in a python
    notebook for iterations and comparisons.

        Inputs:
            sedD14C_df (DataFrame): indexed on Year (A.D.), this dataframe contains columns
            D14C|Fm|depth|mOC and creates Nan-filled columns mOC_out|D14C_out for output
            DataFrame
            mix_time (int): This is the number of years worth of sediment that the organic carbon will
            mix down. In this model, the increments are time based, so this determines how many years
            the carbon will mix downward.
            mix_form (list of floats): Output of either Gauss_mix_down or square_wave functions that
            calculate the amount of carbon transported downward into the yearly deposition below.
            pad_to_year (int): Year prior to 1950 to which you wish to pad the data. This allows deeper
            mixing of the organic carbon without running up against boundary conditions. Called
            internally by create_input_df
            acc_rate (float): The accumulation rate of the core. Set with constants, called internally by
            create_input_df
            POC_productivity (float): The area-normalized productivity rate. Mass of carbon per unit
            time per unit area. Set in constants, called internally by create_input_df
```

```
        alpha (float): Fractionation factor to conversion of POC (leaf litter, peat) to DIC/DOC.
        Default is 1 (no fractionation)
        epsilon (float): Export efficiency. This is the fraction of the mobilized organic carbon that
        is advected horizontally (out of the model system, likely as DIC or CO2) and can be used
        to align model outputs with expectations of DIC export from marshes and mangroves.
        root_shunt (float): Number of years (downcore depth) that roots inject carbon below. This
        effectively skips the number of years of the shunt in the mixing down of organic carbon
        and adds to layers below. For instance, with a mix-down depth of 10 years and a root_shunt
        of 5 years, the year 1850 will take in carbon from the year 1865, and the years 1860-1864
        (inclusive) will not receive anything. Default is 0.

    '''
    #Create input and output dataframes:
    output_sedD14C_df = create_input_df(pad_to_year, sedD14C_df, acc_rate,
POC_productivity)
    debug('Create output DataFrame...')
    debug(output_sedD14C_df.head())

    for ind in output_sedD14C_df.index:
        if (ind-min(output_sedD14C_df.index)) == 0:
            print('\/\/\/ Bottom boundary layer of peat, year' + str(ind) + ' \/\/\/')
            #Calculate export masses from this layer:
            lateral_export_mass = np.multiply(output_sedD14C_df.loc[ind, 'mOC'],
epsilon)  #exported as dissolved or gas form.
            downward_export_mass = 0        #No downward advection - no place to go.
            #Populate the output dataframe:
            output_sedD14C_df.loc[ind, 'mOC_out'] =  output_sedD14C_df.loc[ind, 'mOC'] -
lateral_export_mass
            output_sedD14C_df.loc[ind, 'D14C_out'] = np.multiply(output_sedD14C_df.loc[ind,
'D14C'], alpha)
            output_sedD14C_df.loc[ind, 'OC_export_mass'] = lateral_export_mass
            output_sedD14C_df.loc[ind, 'OC_export_D14C'] =
np.multiply(output_sedD14C_df.loc[ind, 'D14C'], alpha)



        else:
            for z, val in enumerate(mix_time):  #Loop through the fractions stored in mix_time
(output of Gaussian or square wave generator)
                if ind-z >= min(output_sedD14C_df.index):  #Check to make sure no mixing below
bottom boundary layer
                    #print(val)
                    if z == 0:  #If we are at the air-soil interface, new primary production and loss to
layer below
```

```
            print('^^^^^Air-soil interface in year ' + str(ind) + '.^^^^^')
            OC_in = 0
            fraction_new = 0
            #Calculate export masses from this layer (only import is primary productivity at
the surface):
            #lateral transport first (next 2 lines)
            lateral_export_mass = np.multiply(output_sedD14C_df.loc[ind-z, 'mOC'],
epsilon)
            downward_export_mass = np.multiply((output_sedD14C_df.loc[ind-z, 'mOC'] -
lateral_export_mass), val)

            #downward transport first, then lateral transport (increases instabilities!!!!)
            #downward_export_mass = np.multiply(output_sedD14C_df.loc[ind-z, 'mOC'],
val)
            #lateral_export_mass = np.multiply((output_sedD14C_df.loc[ind-z, 'mOC']-
downward_export_mass), epsilon)

            shunted_mass = downward_export_mass
            #Populate the output dataframe, only for air-soil interface layer:
            output_sedD14C_df.loc[ind-z,'mOC_out'] = output_sedD14C_df.loc[ind, 'mOC']
- lateral_export_mass - downward_export_mass   #equation 1
            output_sedD14C_df.loc[ind-z,'D14C_out'] = (1-
fraction_new)*output_sedD14C_df.loc[ind,'D14C'] #Equation 2, effectively, because
fraction_new is set to 0.
            output_sedD14C_df.loc[ind-z, 'OC_export_mass'] =
downward_export_mass  #Equation 3, loss calculated from the mOC input.
            output_sedD14C_df.loc[ind-z, 'OC_export_D14C'] =
output_sedD14C_df.loc[ind,'D14C_out']*alpha   #No fractionation, alpha = 1 (default), Equation
7.
        else:   #Below-ground stock; gain from above, export out, and loss to below
            print('!_______ Layer between air-soil interface and bottom boundary layer, year '
+ str(ind) + '_______!')
            if root_shunt > 0:
                if z < root_shunt:
                    OC_in = 0              #No mass coming from above, shunted through roots.
                if z >= root_shunt:
                    OC_in = shunted_mass    #Once shunted, hand off is between
downward_export_mass and OC_in
            else:
                OC_in = downward_export_mass        #Mass coming from above, calculated in
last loop (hand-off variable).
            if OC_in < 0:
                print("!!!!! INSTABILITY WARNING - OC_in is negative!!!!!")
```

```
                #OC_in = output_sedD14C_df.loc[ind-z+1,'mOC_out']*mix_time[z-1]*(1-
epsilon)   #Middle term of equation 3

                #If lateral transport happens prior to downward transport...
                lateral_export_mass = np.multiply(output_sedD14C_df.loc[ind-z, 'mOC_out'],
epsilon)
                downward_export_mass = np.multiply((output_sedD14C_df.loc[ind-z,
'mOC_out'] - lateral_export_mass), val)

                #If downward transport happens prior to lateral transport:
                #downward_export_mass = np.multiply(output_sedD14C_df.loc[ind-z, 'mOC'],
val)
                #lateral_export_mass = np.multiply((output_sedD14C_df.loc[ind-z, 'mOC']-
downward_export_mass), epsilon)

                #Equation 3 in three steps below, replacing complicated one-line equation above
this line:
                output_sedD14C_df.loc[ind-z, 'mOC_out'] += OC_in - (lateral_export_mass +
downward_export_mass)       #Add from layer above, calculated as OC_in (Equation 3, first
step)
                fraction_new = np.divide(OC_in, (output_sedD14C_df.loc[ind-z,'mOC_out'] +
OC_in))
                if fraction_new > 1:
                   print('fraction_new too high, something broken!')
                if fraction_new < 0:
                   print('fraction_new too low - something broken!')
                #Now calculate the new isotope composition of the layer
                output_sedD14C_df.loc[ind-z, 'D14C_out'] = np.multiply((1-fraction_new),
output_sedD14C_df.loc[ind-z,'D14C_out']) + np.multiply(fraction_new,
output_sedD14C_df.loc[ind-z+1,'D14C_out'])  #Equation 5
                #output_sedD14C_df.loc[ind-z, 'mOC_out'] += -(lateral_export_mass +
downward_export_mass)
                output_sedD14C_df.loc[ind-z, 'OC_export_mass'] += downward_export_mass
#Equation 3
                output_sedD14C_df.loc[ind-z, 'OC_export_D14C'] =
np.multiply(output_sedD14C_df.loc[ind-z,'D14C_out'], alpha)   #No fractionation, alpha = 1
(default), equation 7

return output_sedD14C_df

def plot_confinedmangrove(df, ax, x_value='210Pb_Date'):
   '''
   Plot confinedmangrove data on given axis. Default is by age but can be switched to depth.
   '''
```

```
    #Get rid of nans
    df_nonans = df[~df['210Pb_Date'].isna()]
    ax.plot(
        df_nonans[x_value],
        df_nonans['D14C'],
        mfc='k',
        mec='k',
        markersize=10,
        marker='o',
        linestyle='--',
        color='k'
    )

def plot_openmangrove(df, ax, x_value='210Pb_Date'):
    '''
    Plot openmangrove data on given axis. Default is by age but can be switched to depth.
    '''
    #Get rid of nans
    df_nonans = df[~df['210Pb_Date'].isna()]
    ax.plot(
        df_nonans[x_value],
        df_nonans['D14C'],
        mfc='None',
        mec='k',
        markersize=10,
        marker='o',
        linestyle='--',
        color='k'
    )

def plot_marsh(df, ax, x_value='210Pb_Date'):
    '''
    Plot marsh data on given axis. Default is by age but can be switched to depth.
    '''
    #Get rid of nans
    df_nonans = df[~df['210Pb_Date'].isna()]
    ax.plot(
        df_nonans[x_value],
        df_nonans['D14C'],
        mfc='None',
        mec='k',
        markersize=10,
        marker='s',
        linestyle='--',
```

```
    color='k'
)
```

SENSITIVITY TESTS

The following code is in Jupyter Notebook language (.ipynb extension).

```
# %%
# Import packages, load data files, set constants

import pandas as pd
import numpy as np
import matplotlib.pyplot as plt
from matplotlib import cm
import swamPy as sw

#Turn debugging on by setting sw.DEBUG to True; off by setting it to False:
sw.DEBUG = False

#Set constants from literature
PgOC_global_mangrove = 2e13 #g/yr #From Twilley et al., 1992 as 0.02 Pg/yr, C sequestered in
peat
PgOC_global_saltmarsh = 1.36e14 #g/yr #Calculated from Alongi 2012/2014, Mcleod et al., 2011
- calculated value is 0.136 Pg/yr
area_global_mangrove = 8649500  #ha #Alongi 2020a
area_global_saltmarsh = 5495100 #ha #Alongi 2020a
#total_area = 14144600 #ha - from Alongi 2020a
acc_rate_mangrove = 0.4 #cm/yr #calculated in Schafer 2020
acc_rate_marsh = 0.08-3.5 #cm/yr
saltmarsh_emission = 0.02-0.24*10**15 #g CO2/yr #Pendleton et al., 2012
mangrove_emission = 0.09-0.45*10**15 #g CO2/yr #Pendleton et al., 2012
mangrove_NPP = 1.82*10**7 #g C/ha/yr  #Alongi 2020a
saltmarsh_NPP = 1.78*10**7 #g C/ha/yr  #Alongi 2020a
burrow_max = 100 #cm #Martinetto et al., 2016
root_depth = 100 #cm #McKee et al., 2007

#Load data files
#Atmospheric bomb curve:
bomb_D14C_df=pd.read_csv('NH1_bombcurve.csv')
#marshdatafile
marsh=pd.read_csv('MarshData.csv')
#openmangrovedatafile
openmangrove=pd.read_csv('OpenMangroveData.csv')
#closedmangrovedatafile
confinedmangrove=pd.read_csv('ConfinedMangroveData.csv')
```

```
#TOCfiles
marshTOC=pd.read_csv('SaltMarsh_TOC.csv')
openmangroveTOC=pd.read_csv('OpenMangrove_TOC.csv')
confinedmangroveTOC=pd.read_csv('ConfinedMangrove_TOC.csv')

#Average yearly bomb curve data and plot:
sedD14C_df = sw.annual_avg_bomb_curve(bomb_D14C_df)
plt.plot(bomb_D14C_df['Year_AD'], bomb_D14C_df['D14C_mean'], ls='-', color='k')
plt.plot(sedD14C_df.index, sedD14C_df['D14C'], 'ro', fillstyle='none')
plt.ylabel('$\\Delta^{14}$C$_{NH1}$')
plt.xlabel('Year, A.D.')

# %% [markdown]
# ## Running the model
#
# Now that the model and associated functions are loaded, we can run it. In this example, we chose two constants:
#  ```
# max_prop = 0.25
# mix_depth = 20
# ```
#  These constants set the physics of mangrove and marsh mixing down. They state that the maximum proportion of material mixed downwards will be 0.25 (25%) and that the depth of downward mixing will be 20 years (this is in time, not core depth, because the model is currently built that way). We will pad the data back to 1850 and use some of the constants set in the cell above. Let's see what this looks like.

# %%
#Set the variables listed above:
sw.DEBUG = False
max_prop = 0.2
mix_depth = 25

#Run the mixing model (choose either square wave or Gaussian
#by removing the # from the one you want and putting the # in front of the one you do not want.)
#att_prop = sw.Gauss_mix_down(mix_depth, max_prop)
att_prop = sw.square_wave(mix_depth, max_prop)

#Run the model:
model_output_df = sw.model_interator_time(
   sedD14C_df, att_prop,
   1850,
   acc_rate_mangrove,
   PgOC_global_mangrove/area_global_mangrove,
```

```
    epsilon=0.6,
    root_shunt=0.5*mix_depth
)

# %% [markdown]
# ## Visualize the model output
#
# Now what? The cell above supposedly ran the model, but it did not generate a figure. We do that in the cell below. The default is to plot the index of the dataframe (years) on the x-axis and the isotope composition ($\Delta$<sup>14</sup>C) on the y-axis. you can change this to plot the depth, the amount of organic carbon, the carbon export. Visualization is important and it is equally important not to commit to only one form of visualization - look at the data from different angles!

# %%
#Visualize output from the single run in the cell above:
_, ax = plt.subplots(nrows=1, ncols=1)

v = model_output_df
ax.plot(v.index, v['D14C_out'], c='peru')
title = ('Model output: Mix_depth = ' + str(mix_depth) + 'y, max_prop = ' + str(max_prop))
print(title)
ax.set(title=title, xlabel=r'Year A.D.', ylabel=r'$\Delta$$^{14}$C')

#Add observations
#sw.plot_confinedmangrove(confinedmangrove, ax)
#sw.plot_openmangrove(openmangrove, ax)
sw.plot_marsh(marsh, ax)

# %% [markdown]
# ## Plotting TOC figures
# In the below cell, we will plot the %TOC for each site.

# %%
#plt.plot(sedD14C_df.index, sedD14C_df['D14C'], ls='-', color='k')
plt.plot(marshTOC['210Pb_yr'], marshTOC['OC'], 'ro', fillstyle='none')
#plt.plot(openmangroveTOC['210Pb_yr'], openmangroveTOC['OC'], 'ro', fillstyle='none')
#plt.plot(confinedmangroveTOC['210Pb_yr'], confinedmangroveTOC['OC'], 'ro', fillstyle='none')
plt.xlabel(r'$^{210}$Pb Date')
plt.ylabel('% TOC')

# %% [markdown]
# ## Iterating through different mix down models and constants
#
```

```
# In the next cell, we are going to use the yearly bomb carbon <sup>14</sup>C values as well as some of the constants from the cell above to iterate through different mixing depths and different mixing proportions. This differs from above in that we will use several different mixing depths at the same max_prop. This is `Modeling 101` - change one variable at a time and observe how it affects the comparison to the data! You can change the range of mixing depths and the max_prop to maximize the fit to your observations.
#
# We will observe whether this leads to a better understanding of the observed data and how to make the model approach those data. Do we have control of adequate variables to force the model to fit the data? Or do we need to adjust other variables or even change the modeling approach to achieve fit?

# %%
#Iterate through different mixing depths with both a Gaussian and square wave curve
sw.DEBUG = False
mix_depths = list(map(int, np.linspace(21, 100, 4)))      #This is a list of integers to change downmix depth.\r\n",
print(mix_depths)
max_prop = 0.8
epsilon=0.1

#Gaussian models:
#Create empty dictionaries to store output DataFrames:
output_dict_Gauss = {}
output_dict_square = {}

#Run model for each mix_depth in list:
for depth in list(mix_depths):
    #print(depth)
    att_prop_Gaussian = sw.Gauss_mix_down(depth, max_prop)
    #print(att_prop_Gaussian)
    att_prop_sqwave = sw.square_wave(depth, max_prop)
    #print(att_prop_sqwave)
    model_out_Gauss= sw.model_interator_time(sedD14C_df, att_prop_Gaussian, 1850, acc_rate_mangrove, PgOC_global_mangrove/area_global_mangrove, epsilon=epsilon, root_shunt=0.5*depth)
    model_out_square= sw.model_interator_time(sedD14C_df, att_prop_sqwave, 1850, acc_rate_mangrove, PgOC_global_mangrove/area_global_mangrove, epsilon=epsilon, root_shunt=0.5*depth)
    #update output dictionaries
    output_dict_Gauss |= {str(depth):model_out_Gauss}
    output_dict_square |= {str(depth):model_out_square}
    print(output_dict_Gauss.keys())
```

```
# %%
#Visualize output_dict from cell above:
_, ax = plt.subplots(nrows=2, ncols=1)
colormap = cm.get_cmap('copper', len(output_dict_Gauss))
legend_labels=list([None]*len(output_dict_Gauss))
ctr = 0
#Plot the Gaussian model runs
for k, v in output_dict_Gauss.items():
    ax[0].plot(v.index, v['D14C_out'], c=colormap(ctr))
    legend_labels[ctr] = 'Mix depth = ' + k + ' y'
    ctr = ctr + 1
    ax[0].set(title='Gaussian', ylabel=r'$\Delta$$^{14}$C')
    ax[0].legend(legend_labels)

#Reset counter and plot the square wave
ctr = 0
#Plot the square wave model runs
for k, v in output_dict_square.items():
    ax[1].plot(v.index, v['D14C_out'], c=colormap(ctr))
    ctr = ctr + 1
    ax[1].set(title='Square Wave', xlabel=r'Year A.D.', ylabel=r'$\Delta$$^{14}$C')
    ax[0].tick_params(
        axis='x',          # changes apply to the x-axis
        which='both',      # both major and minor ticks are affected
        bottom=True,      # ticks along the bottom edge are off
        top=False,         # ticks along the top edge are off
        labelbottom=False)

#Add observations
for axis in ax.flatten():
    sw.plot_confinedmangrove(confinedmangrove, axis)
    sw.plot_openmangrove(openmangrove, axis)
    sw.plot_marsh(marsh, axis)

# %% [markdown]
# ## Do we have mass conservation?
#
# To conserve mass, the amount of carbon put into the system must equal that which is left in the system plus that which has left, or bypassed, the system. We track the amount of OC export from the system as well as its isotopic composition. Here, we determine whether mass is conserved by
# 1. Summing the total mass of carbon produced and deposited,
# 2. Summing the total amount of carbon remaining in the core, and
# 3. Summing the total output of carbon from the system.
#
```

```
#  If the second and third bullets add up to the first, we have conserved mass.

# %%
#Set example dataframe from the output dictionary populated by iterative model:
exp_df = output_dict_Gauss['51']

total_production = sum(exp_df['mOC'])              #Bullet 1 above
total_preservation = sum(exp_df['mOC_out'])        #Bullet 2 above
total_export = sum(exp_df['OC_export_mass'])       #Bullet 3 above
print('Total production = ', total_production, '\n', 'Total preservation in core = ',
total_preservation, '\n', 'Total export = ', total_export, '\n')

if total_production - (total_preservation + total_export) == 0:
    print('Conservation of mass acheived!!!')
else:
    print('Womp, womp, conservation of mass not achieved.')
```